EXPERIMENTAL AND COMPUTATIONAL FAILURE ANALYSIS OF GRAPHITE/BISMALEIMIDE LAMINATED COMPOSITE AND CARBON FOAM IN SANDWICH CONSTRUCTION

THESIS

Troy C. Welker, First Lieutenant, USAF

AFIT/GAE/ENY/03-10

DEPARTMENT OF THE AIR FORCE
AIR UNIVERSITY

AIR FORCE INSTITUTE OF TECHNOLOGY

Wright-Patterson Air Force Base, Ohio

AFIT/GAE/ENY/03-10

EXPERIMENTAL AND COMPUTATIONAL FAILURE ANALYSIS OF GRAPHITE/BISMALEIMIDE LAMINATED COMPOSITE AND CARBON FOAM IN SANDWICH CONSTRUCTION

THESIS

Presented to the Faculty

Department of Aeronautics and Astronautics

Graduate School of Engineering and Management

Air Force Institute of Technology

Air University

Air Education and Training Command

in Partial Fulfillment of the Requirements for the

Degree of Master of Science in Aeronautical Engineering

Troy C. Welker, BAEM, MS

First Lieutenant, USAF

March 2003

AFIT/GAE/ENY/03M-10

EXPERIMENTAL AND COMPUTATIONAL FAILURE ANALYSIS OF GRAPHITE/BISMALEIMIDE LAMINATED COMPOSITE AND CARBON FOAM IN SANDWICH CONSTRUCTION

Troy C. Welker, BAEM, MS

First Lieutenant, USAF

Approved:

Professor Anthony N. Palazotto (Chairman)	Date 3-12-03
Dr. Gregory A. Schoeppner (Member)	Date 3-12-03
Lt Col Robert A. Canfield (Member)	Date 3-12-03
Maj Richard G. Cobb (Member)	Date 12 MAR 03

Acknowledgements

This research effort would not have been possible without the support, advice and assistance of Dr. Sangwook Sihn, University of Dayton Research Institute, and Dr. Victor Y. Perel, Air Force Institute of Technology. Dr. Sihn has especially become a friend to me through my first experience in conducting and reporting original experimental research, and he has taught me a lot about the engineering discipline. I look forward to working with him on future efforts.

Thanks to Mr. Mark Derriso, Air Vehicles Directorate, for providing funding for this research. I also thank the Materials and Manufacturing Directorate for the use of the laboratory and related equipment, and John Camping, Ron Esterline, Erik Ripberger, and Ron Trejo from the University of Dayton Research Institute for their assistance in the lab.

During my academic career I have had the privilege of learning from several gifted instructors. I would like to thank two professors specifically, Lt Col Robert A. Canfield from AFIT and Dr. Gordon S. Beavers from the University of Minnesota. Lt Col Canfield's instruction in finite element analysis and his outside-of-class help allowed me to excel in the most challenging course I took at AFIT. Dr. Beavers' unique English wit, style, and excellent instruction of aerospace propulsion and aerodynamics ("finite wing theory for geese") inspired me to study aerospace engineering at the graduate level.

I extend special, heartfelt thanks to Dr. Palazotto for his patience and guidance. Dr. P always had time in class or in his office to give thorough, thoughtful answers to all of my questions, no matter how simple, and used quite a bit of chalk and red ink to help shape this presentation into what you are reading.

Finally, thank you to all my family and friends. I especially thank my wife for all her love and support.

Troy C. Welker

Table of Contents

List of Figures

List of Tables

Abstract

Sandwich beams consisting of a carbon foam core and graphite/bismaleimide face sheets were constructed and tested. Nine specimens were fabricated, using three distinct cross-ply symmetric face sheet layups with a constant core thickness. Four-point bend testing, controlled by a constant rate of midspan vertical displacement, was used to load the specimens to failure. Strains were recorded at midspan on the top and bottom faces, and vertical displacement was measured at midspan. Failure modes were observed for the beams and compared to results from a layerwise finite element method. The finite element code was originally written to dynamically calculate stresses in a sandwich plate dropped on an elastic foundation, and was enhanced to handle concentrated static forces. In addition to in-plane strains and stresses, the finite element method takes into account both normal and shear strains and stresses through the thickness of the beam. The stress results were used to evaluate failure criteria for both the composite face sheets and foam core. Displacements and strains from the experiment were compared to analytical sandwich beam theory, and displacements and failure loads were compared to the finite element solution. A phenomenological failure criterion was developed that compares favorably with experimental failure data. The finite element solution gives failure within an average of 7.58% of experiment, and a stiffness within an average of 11.16%. The analytical sandwich beam theory predicts stiffness within 4.83% of experiment, and strain within 5.27% of experiment. A primary goal of the research was to evaluate the ability of the layerwise finite element method, a method having potential use in a structural health monitoring system, to predict failure onset and location in a structure. Another goal was to determine if the structures responded in such a way that core failure in shear was reinforced by the face sheets. This research shows that the finite element theory has the ability to predict failure onset and location in a sandwich structure, and that the face sheet layups with higher stiffness delay the onset of shear failure in the core.

EXPERIMENTAL AND COMPUTATIONAL FAILURE ANALYSIS OF GRAPHITE/BISMALEIMIDE LAMINATED COMPOSITE AND CARBON FOAM IN SANDWICH CONSTRUCTION

I. Introduction

Sandwich construction in its simplest form consists of sheets of material adhered to either side of a layer of core material. Usually, the core is much thicker and much less dense than the face sheets. This allows the structure to have a greater bending stiffness than a single solid plate of face sheet material having the same weight, the increased stiffness being the result of the face sheets being fixed at a greater distance from the centroidal axis. Sandwich structures of today owe their popularity in large part to their high stiffness-weight and strength-weight ratios.

Sandwich construction was in existence before the advent of modern composite materials. Its earliest use is believed to have been by Sir William Fairbairn in tubular bridge design and construction in Great Britain, and appears in the literature as early as 1849 (as reported in [2]). The idea of sandwich construction had possibly occurred to independent engineers before this time without having been reported or used in the construction of a load-bearing structure.

Two prominent examples of sandwich construction can be found in aviation history. The first extends back to the World War II (WWII) era. The deHavilland aircraft company produced the DH-98 MOSQUITO, flown by Great Britain's Royal Air Force during WWII (Figure 1.1). Its primary structure consisted of balsa core material between exterior and

Figure 1.1 deHavilland DH-98 MOSQUITO [29]

interior plywood sheets. The aircraft entered production in 1941, and production was continued well beyond the war [29].

The second notable example of sandwich construction in aviation history is found in the Apollo space program of the United States' National Aeronautics and Space Administration (NASA). Two concentric sandwich shells consisting of thin steel sheets surrounding cores of lightweight stainless steel honeycomb (exterior shell) and aluminum honeycomb (interior shell) were designed by North American Rockwell Corporation for the construction of the Apollo command module (Figure 1.2). It was critical for the command module to be as lightweight as possible to maximize payload capacity, yet strong enough to withstand reentry into the atmosphere. The outer shell of the vehicle was covered with a phenolic epoxy resin to withstand reentry temperatures of over 1600 °C [29].

In a sandwich structure subjected to a bending load, the thin face sheets usually carry the majority of compressive and tensile stresses. The thick core acts to keep the face sheets parallel to each other and separated from each other by their original distance from the centroidal axis by providing adequate stiffness in the thickness direction of the beam. The core also prevents the face sheets from sliding over each other by providing shear stiffness. Thus, in predicting and analyzing failure of sandwich structures, one must be concerned with the tensile and compressive strengths of the face sheets and the through-

Figure 1.2 North American Rockwell Apollo 15 Command Module

thickness and shear strengths of the core, since the failure will largely depend on those properties.

Carbon foam is an emerging ultralightweight material being used in sandwich beam construction because of its low density and high stiffness and strength. Several applications of carbon foam can be found in all fields of engineering. The advantages of an ultralightweight material are evident when considering the field of advanced aerospace vehicles, where using materials with high stiffness-weight ratios can reduce the weight of the aircraft and allow it to carry more fuel and/or payload. Its efficient thermal management characteristics make it desirable for other structural applications as well, including high-density electronics, hybrid diesel-electric vehicles, rocket combustors, and commu-

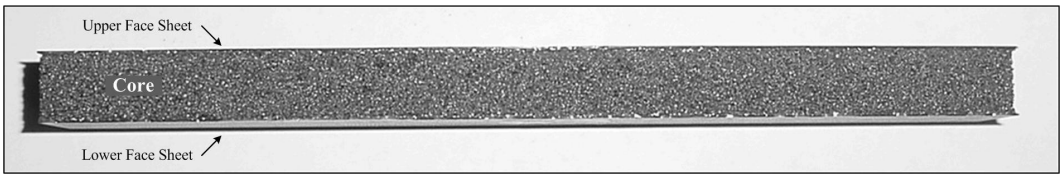

Figure 1.3 Graphite/BMI and Carbon Foam Sandwich Beam

nication satellites [25]. Future applications that take advantage of its high stiffness and strength are currently being researched.

When analyzing load-bearing structures, it is important to be able to detect when their constituent materials are damaged and their high strengths and stiffnesses are degraded. Structural health monitoring, a field of emerging importance, has generated Department of Defense interest in relation to advanced aircraft structures. The goal of a structural health monitoring system is to be able to predict or detect the onset and location of failure in a given structure, preferably in real time, based on known information about the loading conditions and material properties of the structure. This becomes important in composite sandwich structures because the failure may be difficult or impossible to detect using traditional nondestructive inspection techniques.

Structural failure degrades the ability of a structure to respond under loading. This thesis analyzes structural response using three different methods: an analytical approach using beam theory, a computational approach using a finite element solution, and a physical experiment conducted on nine specimens. The analytical method [2] uses an application of ordinary beam theory to consider the effect of sublaminates (face sheets and core) of different materials on bending stiffness of the sandwich structure. The sandwich beam theory considers narrow beams consisting of different isotropic materials for the face sheet and for the core, and was applied to the analysis of the composite face sheets. The results of this theory were compared with the experimental data for load-displacement and load-strain responses.

Failure was studied using both computational and experimental methods. The computational approach to failure analysis, developed by Perel and Palazotto in [17] and [19],

uses a finite element method that considers the effect of through-thickness strain in addition to the in-plane strains, while requiring relatively few degrees of freedom in comparison to a full three-dimensional model and solution. Stresses are obtained through constitutive relations and by solving the equations of motion for the sandwich structure for three zones through its thickness: upper face sheet, core, and lower face sheet. The stresses are then used to compute failure indices to predict failure initiation and mode in each sublaminate.

To physically characterize failure, an experiment was performed with sandwich structures consisting of a carbon foam core between two face sheets of a laminated composite. The carbon foam was obtained from Touchstone Research Laboratory, and its material properties were determined by experiment [24]. The face sheets consist of graphite fibers embedded in bismaleimide (BMI) matrix in the form of preimpregnated rolled tape. The cured composite laminate is stated to have material properties equivalent to those of Cytec CYCOM IM7/5250-4 [5]. Four-point bend tests were performed with each sandwich structure. The specimens were loaded such that the load resulted in a constant rate of midspan displacement, and the loading was carried out until structural failure. A time history of load, top and bottom face sheet strain, and midspan displacement was recorded, and the failure mode for each specimen was noted.

This presentation concludes with the comparison and discussion of the analytical, computational, and experimental results, followed by a summary of findings from this research.

II. Theoretical Foundation

2.1 Theory of Linear Elasticity: Orthotropic and Transversely Isotropic Materials

In order to consider the structural response and failure of the sandwich beams, appropriate theories must be applied to the analysis. This chapter lays the theoretical groundwork for the sandwich beam analysis carried out in this thesis. Composite laminate theory, sandwich beam theory, finite element theory, and failure theory are discussed.

Herakovich [10] and Saada [23] give a full treatment of the three-dimensional constitutive relations for a linear elastic material and the simplifications obtained by the transverse isotropy assumption. A summary of this treatment is presented here for completeness, beginning with the statement that the full fourth-order compliance tensor from the generalized Hooke's law $\varepsilon_{kl} = S_{klmn}\sigma_{mn}$ [23] can be simplified by making assumptions about the independence of direction on effective material properties.

2.1.1 Orthotropic Materials. A material that is symmetric about three orthogonal planes is an orthotropic material. A unidirectional composite lamina can be considered to be orthotropic because it exhibits material symmetry through its thickness, along its fibers, and transverse to its fibers.

The constitutive relations from elasticity theory are presented in Equations 2.1a–2.1f in terms of engineering constants. This is useful because engineering constants are quantities that can be measured in the laboratory. These constants E, G, and ν are the

elasticity modulus (Young's modulus), shear modulus, and Poisson's ratio, respectively.

$$\varepsilon_1 = \frac{1}{E_1}\sigma_1 - \frac{\nu_{21}}{E_2}\sigma_2 - \frac{\nu_{31}}{E_3}\sigma_3 \tag{2.1a}$$

$$\varepsilon_2 = -\frac{\nu_{12}}{E_1}\sigma_1 + \frac{1}{E_2}\sigma_2 - \frac{\nu_{32}}{E_3}\sigma_3 \tag{2.1b}$$

$$\varepsilon_3 = -\frac{\nu_{13}}{E_1}\sigma_1 - \frac{\nu_{23}}{E_2}\sigma_2 + \frac{1}{E_3}\sigma_3 \tag{2.1c}$$

$$\varepsilon_4 = \frac{1}{G_{23}}\sigma_{23} \tag{2.1d}$$

$$\varepsilon_5 = \frac{1}{G_{13}}\sigma_{13} \tag{2.1e}$$

$$\varepsilon_6 = \frac{1}{G_{12}}\sigma_{12}. \tag{2.1f}$$

Here the usual elasticity nomenclature for stress and strain is replaced with a shorthand notation (Equations 2.2–2.3) commonly used in composites literature, with indices $(i, j = 1, 2, \ldots, 6)$. Note that shear strains ε_4, ε_5, and ε_6 are defined as engineering shear strains, double that of the expressions for shear strain in linear elasticity theory.

$$\sigma_1 \equiv \sigma_{11}; \quad \sigma_2 \equiv \sigma_{22}; \quad \sigma_3 \equiv \sigma_{33}; \quad \sigma_4 \equiv \sigma_{23}; \quad \sigma_5 \equiv \sigma_{13}; \quad \sigma_6 \equiv \sigma_{12} \tag{2.2}$$

$$\varepsilon_1 \equiv \varepsilon_{11}; \quad \varepsilon_2 \equiv \varepsilon_{22}; \quad \varepsilon_3 \equiv \varepsilon_{33}; \quad \varepsilon_4 \equiv 2\varepsilon_{23}; \quad \varepsilon_5 \equiv 2\varepsilon_{13}; \quad \varepsilon_6 \equiv 2\varepsilon_{12} \tag{2.3}$$

Figure 2.1 illustrates the material coordinate system used in composite laminate theory.

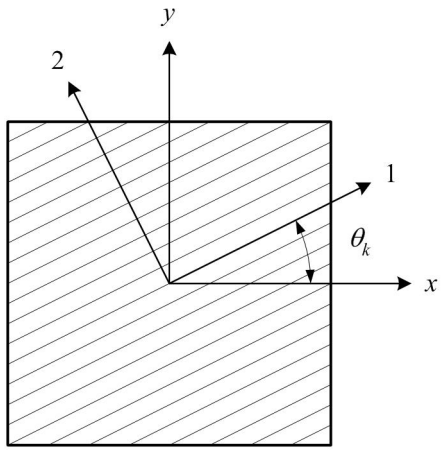

Figure 2.1 Material Coordinate Axis System

The constitutive relations in Equations 2.1a–2.1f can be written in matrix form. The result is the compliance matrix **S**. The constitutive relations then appear as:

$$\begin{Bmatrix} \varepsilon_1 \\ \varepsilon_2 \\ \varepsilon_3 \\ \varepsilon_4 \\ \varepsilon_5 \\ \varepsilon_6 \end{Bmatrix} = \begin{bmatrix} S_{11} & S_{12} & S_{13} & 0 & 0 & 0 \\ S_{12} & S_{22} & S_{23} & 0 & 0 & 0 \\ S_{13} & S_{23} & S_{33} & 0 & 0 & 0 \\ 0 & 0 & 0 & S_{44} & 0 & 0 \\ 0 & 0 & 0 & 0 & S_{55} & 0 \\ 0 & 0 & 0 & 0 & 0 & S_{66} \end{bmatrix} \begin{Bmatrix} \sigma_1 \\ \sigma_2 \\ \sigma_3 \\ \sigma_4 \\ \sigma_5 \\ \sigma_6 \end{Bmatrix}. \tag{2.4}$$

Replacing the compliance terms in Equation 2.4 with the coefficients of the stress terms in Equations 2.1a–2.1f, the constitutive relations can be written in matrix form explicitly

in terms of engineering constants:

$$\begin{Bmatrix} \varepsilon_1 \\ \varepsilon_2 \\ \varepsilon_3 \\ \varepsilon_4 \\ \varepsilon_5 \\ \varepsilon_6 \end{Bmatrix} = \begin{bmatrix} \frac{1}{E_1} & -\frac{\nu_{21}}{E_2} & -\frac{\nu_{31}}{E_3} & 0 & 0 & 0 \\ -\frac{\nu_{12}}{E_1} & \frac{1}{E_2} & -\frac{\nu_{32}}{E_3} & 0 & 0 & 0 \\ -\frac{\nu_{31}}{E_1} & -\frac{\nu_{32}}{E_2} & \frac{1}{E_3} & 0 & 0 & 0 \\ 0 & 0 & 0 & \frac{1}{G_{23}} & 0 & 0 \\ 0 & 0 & 0 & 0 & \frac{1}{G_{13}} & 0 \\ 0 & 0 & 0 & 0 & 0 & \frac{1}{G_{12}} \end{bmatrix} \begin{Bmatrix} \sigma_1 \\ \sigma_2 \\ \sigma_3 \\ \sigma_4 \\ \sigma_5 \\ \sigma_6 \end{Bmatrix}. \tag{2.5}$$

Because the compliance matrix **S** is symmetric, i.e. $S_{ij} = S_{ji}$, the following equalities are observed in the cross-diagonal terms of **S**:

$$\frac{\nu_{21}}{E_2} = \frac{\nu_{12}}{E_1}; \quad \frac{\nu_{31}}{E_3} = \frac{\nu_{13}}{E_1}; \quad \frac{\nu_{32}}{E_3} = \frac{\nu_{23}}{E_2}. \tag{2.6}$$

Thus, the constitutive relations for an orthotropic material can be rewritten by replacing ν_{21}, ν_{31}, and ν_{32} terms in Equation 2.4 with the equalities in Equation 2.6 as follows:

$$\begin{Bmatrix} \varepsilon_1 \\ \varepsilon_2 \\ \varepsilon_3 \\ \varepsilon_4 \\ \varepsilon_5 \\ \varepsilon_6 \end{Bmatrix} = \begin{bmatrix} \frac{1}{E_1} & -\frac{\nu_{12}}{E_1} & -\frac{\nu_{13}}{E_1} & 0 & 0 & 0 \\ -\frac{\nu_{12}}{E_1} & \frac{1}{E_2} & -\frac{\nu_{23}}{E_2} & 0 & 0 & 0 \\ -\frac{\nu_{13}}{E_1} & -\frac{\nu_{23}}{E_2} & \frac{1}{E_3} & 0 & 0 & 0 \\ 0 & 0 & 0 & \frac{1}{G_{23}} & 0 & 0 \\ 0 & 0 & 0 & 0 & \frac{1}{G_{13}} & 0 \\ 0 & 0 & 0 & 0 & 0 & \frac{1}{G_{12}} \end{bmatrix} \begin{Bmatrix} \sigma_1 \\ \sigma_2 \\ \sigma_3 \\ \sigma_4 \\ \sigma_5 \\ \sigma_6 \end{Bmatrix}. \tag{2.7}$$

2.1.2 Transversely Isotropic Materials. When a material has properties independent of coordinate direction in one of its planes, it is said to be transversely isotropic. Assume, for instance, that the plane of isotropy is the 23-plane. Since the material's properties are independent of coordinate direction in this plane, the 2- and 3-directions are equivalent, i.e. $E_2 = E_3$, $\nu_{12} = \nu_{13}$, and $G_{12} = G_{13}$. Also, Equation 2.8 holds for the

23-plane of isotropy:

$$G_{23} = \frac{E_2}{2(1+\nu_{23})}. \tag{2.8}$$

The preceding equalities can be used to write the constitutive matrix equation for a transversely isotropic material in the form of Equation 2.9, again explicitly in terms of engineering constants:

$$\begin{Bmatrix} \varepsilon_1 \\ \varepsilon_2 \\ \varepsilon_3 \\ \varepsilon_4 \\ \varepsilon_5 \\ \varepsilon_6 \end{Bmatrix} = \begin{bmatrix} \frac{1}{E_1} & -\frac{\nu_{12}}{E_1} & -\frac{\nu_{12}}{E_1} & 0 & 0 & 0 \\ -\frac{\nu_{12}}{E_1} & \frac{1}{E_2} & -\frac{\nu_{23}}{E_2} & 0 & 0 & 0 \\ -\frac{\nu_{12}}{E_1} & -\frac{\nu_{23}}{E_2} & \frac{1}{E_2} & 0 & 0 & 0 \\ 0 & 0 & 0 & \frac{2(1+\nu_{23})}{E_2} & 0 & 0 \\ 0 & 0 & 0 & 0 & \frac{1}{G_{12}} & 0 \\ 0 & 0 & 0 & 0 & 0 & \frac{1}{G_{12}} \end{bmatrix} \begin{Bmatrix} \sigma_1 \\ \sigma_2 \\ \sigma_3 \\ \sigma_4 \\ \sigma_5 \\ \sigma_6 \end{Bmatrix}. \tag{2.9}$$

2.2 Composite Laminate Theory

In order to determine the effective elastic and shear moduli for the face sheets, laminate theory is used. Agarwal [1], Herakovich [10], and Whitney [30] describe this theory in detail. It is useful to determine effective engineering constants for a composite laminate so one can compare laminates to other materials or select materials for structural design purposes. Presented here is the application of laminate theory to determine the effective spanwise elastic moduli of the face sheets. The presentation follows the aforementioned references, notably [10].

Laminate theory is based on the plane stress assumption, that is, all through-thickness stresses in the laminate are considered irrelevant. For most problems, this is acceptable because the thickness dimension of the laminate is usually orders of magnitude less than either the span or width dimensions, which carry most of the stress.

Starting with the constitutive relations for an orthotropic material in Equation 2.4, the stress-strain relationship for a composite lamina in a plane stress condition can be

simplified to:

$$\begin{Bmatrix} \varepsilon_1 \\ \varepsilon_2 \\ \varepsilon_6 \end{Bmatrix} = \begin{bmatrix} S_{11} & S_{12} & 0 \\ S_{21} & S_{22} & 0 \\ 0 & 0 & S_{66} \end{bmatrix} \begin{Bmatrix} \sigma_1 \\ \sigma_2 \\ \sigma_6 \end{Bmatrix}. \tag{2.10}$$

Inverting this relationship, we obtain

$$\begin{Bmatrix} \sigma_1 \\ \sigma_2 \\ \sigma_6 \end{Bmatrix} = \begin{bmatrix} Q_{11} & Q_{12} & 0 \\ Q_{21} & Q_{22} & 0 \\ 0 & 0 & Q_{66} \end{bmatrix} \begin{Bmatrix} \varepsilon_1 \\ \varepsilon_2 \\ \varepsilon_6 \end{Bmatrix}. \tag{2.11}$$

where **Q** is known as the reduced stiffness matrix. It is important to note, however, that the terms of the reduced stiffness matrix **Q** are not equal to the corresponding terms of the stiffness matrix **C** from elasticity theory. This relationship is fully developed in [23] and [10]. The reduced stiffness matrix terms Q_{ij} can be written in terms of the compliance matrix terms S_{ij} as follows, using the fact that $\mathbf{Q} = \mathbf{S}^{-1}$:

$$Q_{11} = \frac{S_{22}}{S_{11}S_{22} - S_{12}^2}; \quad Q_{22} = \frac{S_{11}}{S_{11}S_{22} - S_{12}^2}; \quad Q_{12} = \frac{-S_{12}}{S_{11}S_{22} - S_{12}^2}; \quad Q_{66} = \frac{1}{S_{66}}. \tag{2.12}$$

Q_{ij} can also be expressed in terms of the lamina engineering constants as follows:

$$Q_{11} = \frac{E_1}{1 - \nu_{12}^2 \frac{E_2}{E_1}} \tag{2.13a}$$

$$Q_{12} = \frac{\nu_{12} E_2}{1 - \nu_{12}^2 \frac{E_2}{E_1}} \tag{2.13b}$$

$$Q_{21} = Q_{12} \tag{2.13c}$$

$$Q_{22} = \frac{E_2}{1 - \nu_{12}^2 \frac{E_2}{E_1}} \tag{2.13d}$$

$$Q_{66} = G_{12}. \tag{2.13e}$$

The stiffness matrix elements Q_{16}, Q_{61} Q_{26}, and Q_{62} are zero in symmetric laminates because these laminates do not exhibit shear coupling. Whitney develops the stiffness ma-

trix for unbalanced laminates in [30]. In practice, unbalanced laminates are not normally fabricated because during the cooling process, residual thermal stresses cause laminate warping.

For an off-axis lamina with fiber orientation θ_k, a coordinate transformation is necessary to express the lamina reduced stiffness matrix in global coordinates. This transformed stiffness matrix is $\bar{\mathbf{Q}}$ and its elements take the form of Equations 2.14a–2.14f, with $m = \cos\theta_k$ and $n = \sin\theta_k$:

$$\bar{Q}_{11} = Q_{11}m^4 + 2(Q_{12} + 2Q_{66})m^2n^2 + Q_{22}n^4 \tag{2.14a}$$

$$\bar{Q}_{12} = (Q_{11} + Q_{22} - 4Q_{66})m^2n^2 + Q_{12}(m^4 + n^4) \tag{2.14b}$$

$$\bar{Q}_{22} = Q_{11}n^4 + 2(Q_{12} + 2Q_{66})m^2n^2 + Q_{22}m^4 \tag{2.14c}$$

$$\bar{Q}_{16} = [(Q_{11} - Q_{12} - 2Q_{66})m^2 + (Q_{12} - Q_{22} + 2Q_{66})n^2]mn \tag{2.14d}$$

$$\bar{Q}_{26} = [(Q_{11} - Q_{12} - 2Q_{66})n^2 + (Q_{12} - Q_{22} + 2Q_{66})m^2]mn \tag{2.14e}$$

$$\bar{Q}_{66} = (Q_{11} + Q_{22} - 2Q_{12} - 2Q_{66})m^2n^2 + Q_{66}(m^4 + n^4). \tag{2.14f}$$

Only cross-ply laminates are considered in this thesis, therefore the above expressions can be simplified and expressed in matrix form as:

$$\bar{\mathbf{Q}}^{0^\circ} = \begin{bmatrix} \frac{E_1}{1-\nu_{12}^2\frac{E_2}{E_1}} & \frac{\nu_{12}E_2}{1-\nu_{12}^2\frac{E_2}{E_1}} & 0 \\ \frac{\nu_{12}E_2}{1-\nu_{12}^2\frac{E_2}{E_1}} & \frac{E_2}{1-\nu_{12}^2\frac{E_2}{E_1}} & 0 \\ 0 & 0 & G_{12} \end{bmatrix} \tag{2.15}$$

$$\bar{\mathbf{Q}}^{90^\circ} = \begin{bmatrix} \frac{E_2}{1-\nu_{12}^2\frac{E_2}{E_1}} & \frac{\nu_{12}E_2}{1-\nu_{12}^2\frac{E_2}{E_1}} & 0 \\ \frac{\nu_{12}E_2}{1-\nu_{12}^2\frac{E_2}{E_1}} & \frac{E_1}{1-\nu_{12}^2\frac{E_2}{E_1}} & 0 \\ 0 & 0 & G_{12} \end{bmatrix}. \tag{2.16}$$

Laminate theory considers the effect of laminae of distinct fiber orientation θ_k cured together in a specific stacking sequence. The constitutive relations for a laminate can be expressed as follows:

$$\begin{Bmatrix} N \\ M \end{Bmatrix} = \begin{bmatrix} \mathbf{A} & \mathbf{B} \\ \mathbf{B} & \mathbf{D} \end{bmatrix} \begin{Bmatrix} \varepsilon^0 \\ \kappa \end{Bmatrix}, \tag{2.17}$$

where **A**, **B**, and **D** are known as the laminate in-plane stiffness, bending-stretching coupling and bending stiffness matrices, respectively. $\{N\}$ is the in-plane force per unit length, $\{M\}$ is the bending moment per unit length, $\{\varepsilon^0\}$ is the laminate strain at the midplane and $\{\kappa\}$ is the laminate curvature. $\{\varepsilon^0\}$ and $\{\kappa\}$ are associated with the laminate and are not functions of the depth coordinate z.

A, **B**, and **D** are defined in terms of the lamina reduced stiffness matrices as follows:

$$\mathbf{A} = \sum_{k=1}^{N} [\bar{\mathbf{Q}}]^k (z_k - z_{k-1}) \tag{2.18a}$$

$$\mathbf{B} = \frac{1}{2} \sum_{k=1}^{N} [\bar{\mathbf{Q}}]^k (z_k^2 - z_{k-1}^2) \tag{2.18b}$$

$$\mathbf{D} = \frac{1}{3} \sum_{k=1}^{N} [\bar{\mathbf{Q}}]^k (z_k^3 - z_{k-1}^3). \tag{2.18c}$$

where z is the distance from the laminate midplane along the depth coordinate and k is the ply number, as depicted in Figure 2.2. The z-axis in laminate theory is conventionally regarded as being positive downward, and plies are conventionally numbered in sequence from top ply ($-z$) to bottom ply ($+z$). If one deals exclusively with symmetric laminates, $\mathbf{B} = \mathbf{0}$ and the in-plane response is decoupled from the bending response.

$$\{N\} = \mathbf{A}\{\varepsilon^0\} \tag{2.19a}$$

$$\{M\} = \mathbf{D}\{\kappa\}. \tag{2.19b}$$

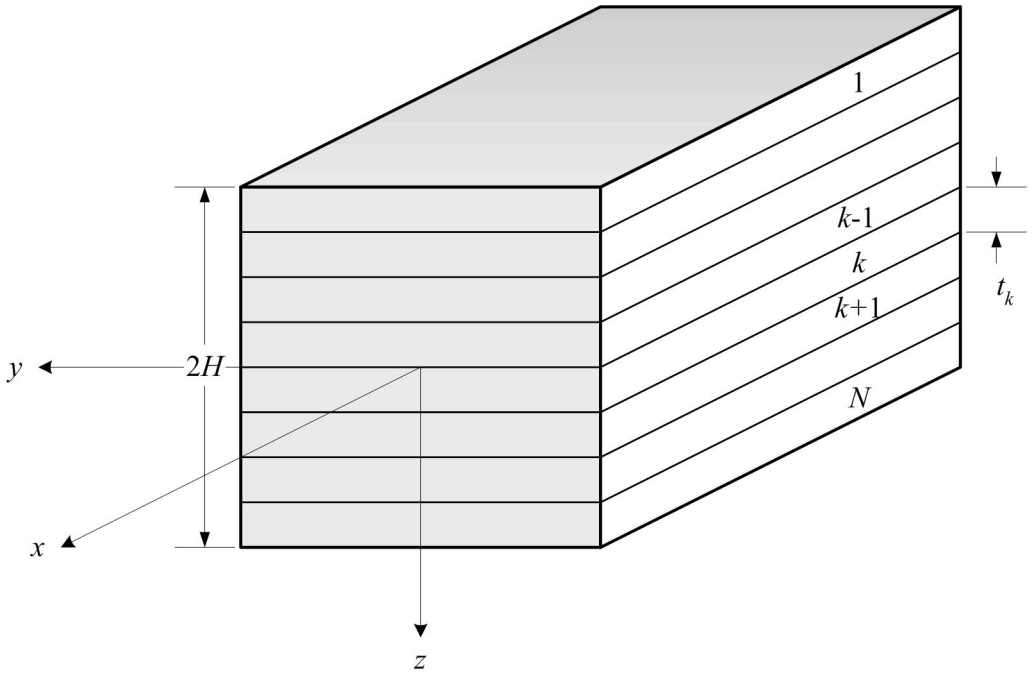

Figure 2.2 Composite Laminate Nomenclature

Therefore, in symmetric laminates, in-plane and bending response can be considered separately. Effective laminate engineering constants are obtained from the laminate in-plane stiffness matrix **A**. The following method of determining laminate engineering constants presented here follows [10].

First, one must define the laminate average stress over the laminate thickness $2H$. This can be represented as follows:

$$\{\bar{\sigma}\} \equiv \frac{1}{2H}\{N\} = \frac{1}{2H}\mathbf{A}\{\varepsilon^0\}. \tag{2.20}$$

Inverting this relationship gives midplane strain as a function of average applied stress:

$$\{\varepsilon^0\} = 2H\mathbf{A}^{-1}\{\bar{\sigma}\}. \tag{2.21}$$

One can define a new quantity $\mathbf{a}^*$, the laminate compliance matrix, as:

$$\mathbf{a}^* \equiv 2H\mathbf{A}^{-1}, \tag{2.22}$$

whereby the laminate constitutive relations can be expressed in general form as:

$$\begin{Bmatrix} \varepsilon_1^0 \\ \varepsilon_2^0 \\ \varepsilon_6^0 \end{Bmatrix} = \begin{bmatrix} a_{11}^* & a_{12}^* & a_{16}^* \\ a_{12}^* & a_{22}^* & a_{26}^* \\ a_{16}^* & a_{26}^* & a_{66}^* \end{bmatrix} \begin{Bmatrix} \bar{\sigma}_1 \\ \bar{\sigma}_2 \\ \bar{\sigma}_6 \end{Bmatrix}. \tag{2.23}$$

Now, similar to the method used to obtain Equation 2.5, elements of the laminate compliance matrix are expressed in terms of engineering constants; however, in the following representation the engineering constants are the effective engineering constants for the entire laminate. For a symmetric laminate:

$$\begin{Bmatrix} \varepsilon_1^0 \\ \varepsilon_2^0 \\ \varepsilon_6^0 \end{Bmatrix} = \begin{bmatrix} \frac{1}{E_x} & -\frac{\nu_{xy}}{E_x} & 0 \\ -\frac{\nu_{xy}}{E_x} & \frac{1}{E_y} & 0 \\ 0 & 0 & \frac{1}{G_{xy}} \end{bmatrix} \begin{Bmatrix} \bar{\sigma}_1 \\ \bar{\sigma}_2 \\ \bar{\sigma}_6 \end{Bmatrix}. \tag{2.24}$$

This expression can now be written in terms of reduced stiffnesses by inverting the constitutive relationship and solving for the engineering constants. Since there is no shear coupling, the engineering constants simplify to:

$$E_x = \bar{Q}_{11} - \frac{\bar{Q}_{12}^2}{\bar{Q}_{22}}, \quad E_y = \bar{Q}_{22} - \frac{\bar{Q}_{12}^2}{\bar{Q}_{11}}, \quad G_{xy} = \bar{Q}_{66}, \quad \nu_{xy} = \frac{\bar{Q}_{12}}{\bar{Q}_{22}}. \tag{2.25}$$

For the sandwich beam theory given in this presentation, the spanwise effective engineering constant E_x is used for the face sheets because the majority of the in-plane stress is in the spanwise direction.

2.3 Sandwich Beam Theory

A sandwich beam theory is developed by Allen [2] that considers the fact that the face sheets and core have distinct material properties. This theory is used to validate experimental results for midspan displacement of a sandwich beam and strain on its upper and lower face sheets, similar to the procedure in [24]. The theory is an extension of elementary beam theory, which states that plane cross sections of a beam remain plane under pure bending.

For an isotropic beam, the relation between bending moment and curvature can be expressed as follows:

$$\frac{M}{EI} = -\frac{1}{R}, \tag{2.26}$$

where M corresponds to bending moment and R to the radius of curvature. The term EI, known as flexural rigidity, determines the degree of flexure of the beam under pure bending, and for isotropic beams is calculated by multiplying the stiffness modulus E by the area moment of inertia of the cross section of the beam I. However, for a sandwich beam consisting of two distinct materials, the effect on flexural rigidity by each constituent must be considered. The expression for flexural rigidity is represented in Equation 2.27. For convenience, and to distinguish flexural rigidity for a sandwich beam from that of a homogeneous beam, the symbol D is used.

$$D = E_{\mathrm{f}}\frac{bt^3}{6} + E_{\mathrm{f}}\frac{btd^2}{2} + E_{\mathrm{c}}\frac{bc^3}{12}, \tag{2.27}$$

The above expression for flexural rigidity consists of three terms. The dimensions b, c, t, and h represent the width of the beam, thickness of the core, thickness of one face sheet, and total beam thickness, respectively. The dimension d is the distance between the midplanes of the upper and lower face sheets: $d = (h+c)/2$, or equivalently $d = t+c$. These expressions assume face sheets of equal thickness. The first term of Equation 2.27 represents the flexural rigidity of the face sheets about their own axes. Since the face sheets have a rectangular cross section, each face sheet contributes a flexural rigidity of its

stiffness E_f times its area moment of inertia, $bt^3/12$. This product is doubled to give the flexural rigidity contribution of both face sheets. The second term represents the flexural rigidity of the face sheets about the sandwich centroidal axis. As a result of invoking the parallel axis theorem [28], the flexural rigidity term for each face sheet also includes E_f times the product of the face sheet cross sectional area and the square of the distance between the centroidal axis of the face sheet and that of the sandwich beam, $btd^2/4$. The third term represents the flexural rigidity of the core—the product of the core stiffness E_c and its area moment of inertia. As it also has a rectangular cross section, its area moment of inertia is $bc^3/12$, similar to that of the face sheet, but since its centroidal axis is coincident with the centroidal axis of the sandwich beam, there is no additional area moment term due to axis offset.

The second term in Equation 2.27 is the dominant term because of the high stiffness of the face sheets relative to the core and their distance from the centroidal axis of the sandwich beam.

From isotropic beam theory [22], the exact solution for midspan displacement of a sandwich beam due to a four-point bending load is expressed as:

$$w_1 = \frac{Pa}{48EI}(3L^2 - 4a^2), \tag{2.28}$$

where P is the total load on the beam such that each point load at the midsurface of the beam is equal to $P/2$, a is the distance between the support and the load (symmetric loading is assumed, see Figure 2.3), EI is the flexural rigidity of the beam, and L is the beam support span. For $a = L/4$, the equation becomes:

$$w_1 = \frac{11PL^3}{768D}. \tag{2.29}$$

In addition to bending moment, shear forces in the sandwich structure contribute to midspan displacement, primarily in the core. It is reasonable to assume that the shear force is constant through the thickness of the core because of the high stiffness of the face sheets

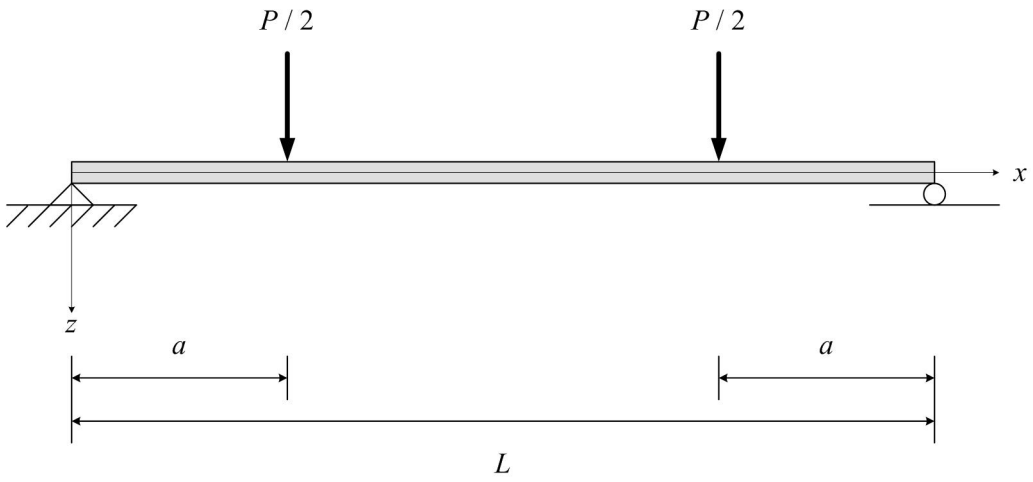

Figure 2.3 Four Point Bending of an Isotropic Beam

relative to the core. The shear stress that results is of the form $\tau = Q/bd$, and is associated with the shear strain $\gamma = Q/Gbd$. In a four-point bend scenario, the shear strain is constant in the region between the support and the load, and is equal to $\gamma = P/2Gbd$. According to Allen [2], this shear strain is not quite equal to the slope of the vertical displacement, as shown in Figure 2.4.

Thus, the differential equation for the vertical displacement contribution due to shear is expressed as:

$$\frac{\mathrm{d}w_2}{\mathrm{d}x} = \gamma\frac{c}{d} = \frac{Pc}{2Gbd^2}. \tag{2.30}$$

In our scenario, shear strain is constant from $0 \leq x \leq L/4$ and zero from $L/4 \leq x \leq L/2$, so the vertical displacement at the midspan due to shear is:

$$w_2 = \frac{Pc}{2Gbd^2} \cdot \frac{L}{4} = \frac{PLc}{8G_c bd^2}, \tag{2.31}$$

where $G = G_c$, the shear modulus of the core. This consideration is based on the assumption that the core carries all of the shear stress. Midspan displacement of the beam can thus be approximated by superimposing displacement due to both bending and shear, as

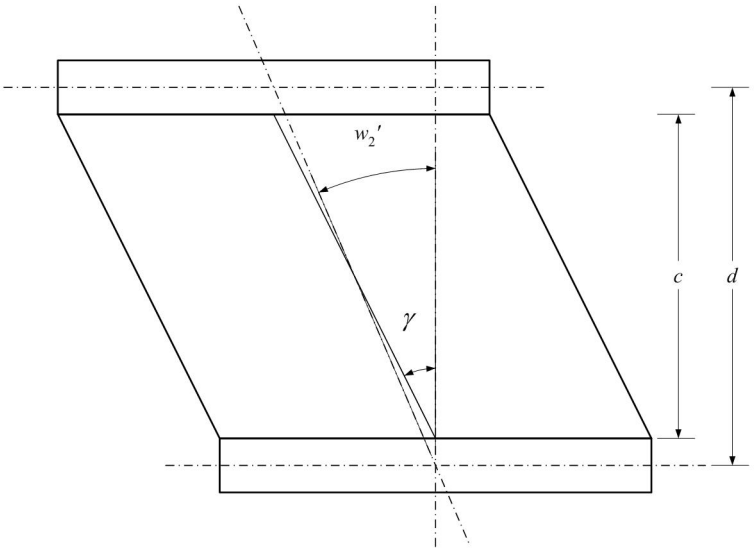

Figure 2.4 Shear Deformation of a Beam With Thick Faces

follows:

$$\delta = \delta_{\text{bending}} + \delta_{\text{shear}} = w_1 + w_2 = \frac{11PL^3}{768D} + \frac{PL}{8(GA)_{\text{eq}}}, \tag{2.32}$$

where

$$(GA)_{\text{eq}} = G_{\text{c}}\frac{bd^2}{c}. \tag{2.33}$$

In this consideration, the core properties G_{c} and E_{c} are obtained from experimental data.

Normal strain in the face sheets at the midspan of the beam is approximated by:

$$\varepsilon_x = \pm\frac{Mh}{2D} = \pm\frac{PLh}{16D}, \tag{2.34}$$

where the upper face sheet is subjected to negative (compressive) strain and the lower face sheet is subjected to positive (tensile) strain. Maximum stress in the core for the four-point bending scenario is approximated by:

$$\tau = \frac{P}{2bd}. \tag{2.35}$$

2.4 Layerwise Theory of Finite Element Analysis

The finite element method used in this presentation is the work of Perel and Palazotto [17], [19]. Perel gives the complete development of this method in [17]. This section is a summary of the layerwise finite element formulation used for the present study.

Perel and Palazotto develop a geometrically nonlinear theory for a thick sandwich plate based on the fact that through-thickness strains play a significant role in the finite element calculations due to the high thickness to length ratio, thickness of the face sheets, and difference in magnitude between the material properties of the face sheets and the core. The theory is based on a layerwise model consisting of three sublaminates: lower face sheet, core, and upper face sheet.

The following assumptions are made in the layerwise theory in both the core and the face sheets [16]:

- Transverse displacement varies in the thickness direction (the core and face sheets are both transversely flexible),
- In-plane displacements vary nonlinearly,
- Transverse shear strain ε_{xz} and transverse normal strain ε_{zz} are taken into account,
- Transverse shear stress σ_{xz} and transverse normal stress σ_{zz} are computed by integration of pointwise nonlinear equations of motion,
- Nonlinear strain-displacement relations are used in order to take account of moderately large displacements and rotations.

The primary unknown functions of the finite element problem for a sandwich plate in cylindrical bending are:

$$u_0, \quad v_0, \quad w_0, \quad \varepsilon_{xz}^{(k)}, \quad \varepsilon_{yz}^{(k)}, \quad \varepsilon_{zz}^{(k)}, \tag{2.36}$$

where $(k = 1,2,3)$ are the sandwich panel zones corresponding to lower face sheet, core, and upper face sheet, in that order, and displacement is at the midsurface of the plate.

Each element consists of two nodes, at finite element coordinates $x = 0$ and $x = l$, respectively. The formulation will begin with all degrees of freedom and nonlinearity taken into account, and will be simplified to the form it appears in the finite element solution considered in this thesis.

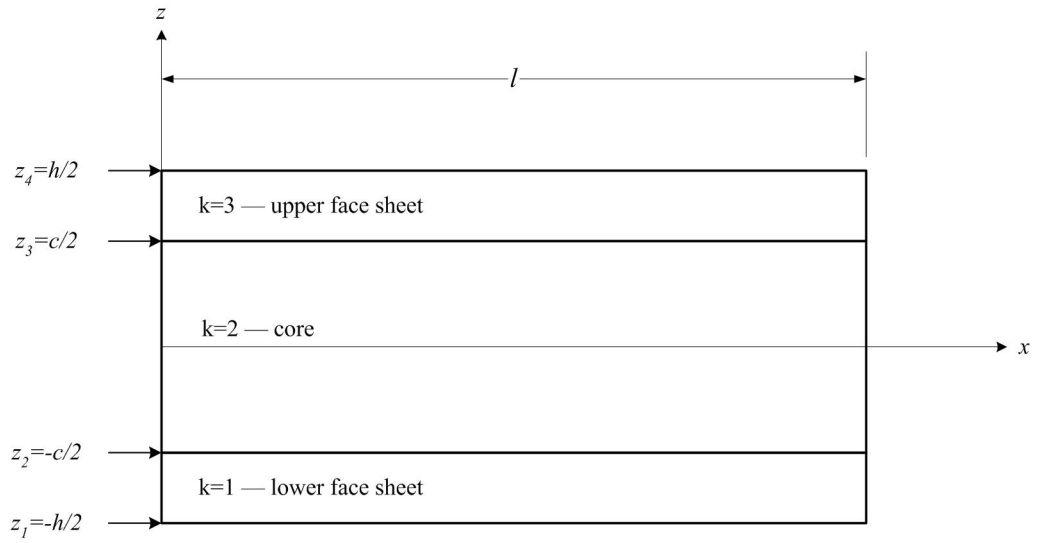

Figure 2.5 Sandwich Plate Coordinate System and Notations

To formulate the finite element, one begins with the following strain-displacement relationships:

$$\varepsilon_{xx} = u_{,x} + \frac{1}{2}(w_{,x})^2 \tag{2.37a}$$

$$\varepsilon_{yy} = v_{,y} + \frac{1}{2}(w_{,y})^2 \tag{2.37b}$$

$$\varepsilon_{xy} = \frac{1}{2}(u_{,y} + v_{,x} + w_{,x}w_{,y}) \tag{2.37c}$$

$$\varepsilon_{xz} = \frac{1}{2}(u_{,z} + w_{,x}) \tag{2.37d}$$

$$\varepsilon_{yz} = \frac{1}{2}(v_{,z} + w_{,y}) \tag{2.37e}$$

$$\varepsilon_{zz} = w_{,z}, \tag{2.37f}$$

where the subscripted comma notation is used to indicate partial derivatives with respect to the variable following the comma. The strain-displacement relationships above, known

as the von Karman relationships, are geometrically nonlinear, that is, the expressions for strain are expressed in higher than first order terms of displacement. If one is interested in only the linear part of the solution because of the small displacements and small rotations involved in the particular problem under consideration, the second-order terms can be set equal to zero. This simplification is made hereafter in this analysis.

For a wide sandwich plate, the plane strain condition is assumed, thus all degrees of freedom in the *y*-coordinate direction vanish, allowing for the unknowns v, ε_{yy}, ε_{xy}, and ε_{yz} to be removed. Also, displacements u and w become functions only of x and z. The unknown functions are then reduced to:

$$u_0, \quad w_0, \quad \varepsilon_{xz}^{(1)}, \quad \varepsilon_{zz}^{(1)}, \quad \varepsilon_{xz}^{(2)} \quad \varepsilon_{zz}^{(2)}, \quad \varepsilon_{xz}^{(3)}, \quad \varepsilon_{zz}^{(3)}. \tag{2.38}$$

The development is continued by expressing the functions for displacement in each of the three zones. These displacements can be expressed using the strain-displacement relationships in Equations 2.37a–2.37f as follows:

$$w_{,z}^{(k)}(x,z) = \varepsilon_{zz}^{(k)} \tag{2.39a}$$

$$u_{,z}^{(k)}(x,z) = 2\varepsilon_{xz}^{(k)} - w_{,x}^{(k)}. \tag{2.39b}$$

These expressions are integrated along the *z*-coordinate (*i.e.* in the thickness direction) to solve for the displacement functions in each zone:

$$w^{(1)} = w_0 + \varepsilon_{zz}^{(2)} z_2 + \varepsilon_{zz}^{(1)}(z - z_2) \tag{2.40a}$$

$$w^{(2)} = w_0 + \varepsilon_{zz}^{(2)} z \tag{2.40b}$$

$$w^{(3)} = w_0 + \varepsilon_{zz}^{(2)} z_2 + \varepsilon_{zz}^{(3)}(z - z_3) \tag{2.40c}$$

$$u^{(1)} = u_0 + (2\varepsilon_{xz}^{(2)} - w_{0,x}) z_2 + (2\varepsilon_{xz}^{(1)} - w_{0,x})(z - z_2) \tag{2.40d}$$

$$u^{(2)} = u_0 + (2\varepsilon_{xz}^{(2)} - w_{0,x}) z \tag{2.40e}$$

$$u^{(3)} = u_0 + (2\varepsilon_{xz}^{(2)} - w_{0,x}) z_3 + (2\varepsilon_{xz}^{(3)} - w_{0,x})(z - z_3), \tag{2.40f}$$

where $w^{(k)}$ and $u^{(k)}$ are the displacements along the z- and x-coordinate directions, respectively, in the face sheets ($k = 1, 3$) and core ($k = 2$). The zero subscripts w_0 and u_0 indicate displacements at the midspan ($z = 0$).

Next, the strains can be expressed in terms of the unknown functions in each sublaminate zone by substituting the displacement functions into the strain-displacement relationships in Equations 2.37a–2.37f. The expressions for strain are presented in [19].

The interpolation polynomials (shape functions) selected for this finite element are obtained from the virtual work principle, and are of sufficient order to ensure continuity of the degrees of freedom at the element boundaries:

$$u_0 = \lfloor M_1 \; M_2 \rfloor \begin{Bmatrix} u(0) \\ u(l) \end{Bmatrix}, \tag{2.41a}$$

$$\varepsilon_{xz}^{(k)} = \lfloor M_1 \; M_2 \rfloor \begin{Bmatrix} \varepsilon_{xz}^{(k)}(0) \\ \varepsilon_{xz}^{(k)}(l) \end{Bmatrix}, \tag{2.41b}$$

where

$$M_1 = 1 - \frac{x}{l}, \quad M_2 = \frac{x}{l}, \tag{2.42}$$

and

$$w_0 = \lfloor N_1 \; N_2 \; N_3 \; N_4 \rfloor \begin{Bmatrix} w_0(0) \\ \frac{\mathrm{d}w_0}{\mathrm{d}x}(0) \\ w_0(l) \\ \frac{\mathrm{d}w_0}{\mathrm{d}x}(l) \end{Bmatrix}, \tag{2.43a}$$

$$\varepsilon_{zz}^{(k)} = \lfloor N_1 \; N_2 \; N_3 \; N_4 \rfloor \begin{Bmatrix} \varepsilon_{zz}^{(k)}(0) \\ \frac{\mathrm{d}\varepsilon_{zz}^{(k)}}{\mathrm{d}x}(0) \\ \varepsilon_{zz}^{(k)}(l) \\ \frac{\mathrm{d}\varepsilon_{zz}^{(k)}}{\mathrm{d}x}(l) \end{Bmatrix}, \tag{2.43b}$$

where

$$N_1 = 1 - \frac{3x^2}{l^2} + \frac{2x^3}{l^3}, \quad N_2 = x - \frac{2x^2}{l} + \frac{x^3}{l^2}, \quad N_3 = \frac{3x^2}{l^2} - \frac{2x^3}{l^3}, \quad N_4 = -\frac{x^2}{l} + \frac{x^3}{l^2}. \tag{2.44}$$

The functions M are first-order Lagrangian interpolation functions, and the functions N are third-order Hermitian interpolation functions. This is developed fully in [19].

Therefore, the combined element has 24 degrees of freedom. The following 12 degrees of freedom are present at each node:

$$u_0,\ \varepsilon_{xz}^{(1)},\ \varepsilon_{xz}^{(2)},\ \varepsilon_{xz}^{(3)},\ w_0,\ \frac{\mathrm{d}w_0}{\mathrm{d}x},\ \varepsilon_{zz}^{(1)},\ \frac{\mathrm{d}\varepsilon_{zz}^{(1)}}{\mathrm{d}x},\ \varepsilon_{zz}^{(2)},\ \frac{\mathrm{d}\varepsilon_{zz}^{(2)}}{\mathrm{d}x},\ \varepsilon_{zz}^{(3)},\ \frac{\mathrm{d}\varepsilon_{zz}^{(3)}}{\mathrm{d}x}. \tag{2.45}$$

These degrees of freedom are reduced by making two simplifying assumptions about the problem. First, it is assumed that, because the face sheets are usually thin in comparison to the core, the displacements and strains in the face sheets can be neglected. This allows us to remove the degrees of freedom with the (1) and (3) superscripts. Second, we remove spanwise displacement from our consideration of the sandwich, as the load will be imposed in the z-coordinate direction and we are primarily interested in the strains and stresses in this through-thickness direction. This results in the following 5 nodal degrees of freedom, presented in the order in which they are established in the finite element code:

$$w_0,\ \frac{\mathrm{d}w_0}{\mathrm{d}x},\ \varepsilon_{xz}^{(2)},\ \varepsilon_{zz}^{(2)},\ \frac{\mathrm{d}\varepsilon_{zz}^{(2)}}{\mathrm{d}x}. \tag{2.46}$$

These degrees of freedom are then substituted into the classic equation of finite element analysis $[k]\{d\} = \{r\}$. This equation is solved for the unknown degrees of freedom, imposing the displacement and force boundary conditions according to the problem of interest. While it is possible using the theory developed by Perel and Palazotto to consider a time-dependent problem with geometric nonlinearities present, the simplifications above assume a linear static solution, which is valid for the low loading rate and small displacements considered in this thesis.

Once the displacements and strains are found, the stresses are obtained in a post-processing stage. The in-plane stresses are calculated for each sublaminate zone from the constitutive relations obtained from elasticity theory, which are as follows for the case of cylindrical bending:

$$\sigma_{xx}^{(k)} = \frac{E^{(k)}}{(1+\nu^{(k)})(1-2\nu^{(k)})}[(1-\nu^{(k)})\varepsilon_{xx}^{(k)} + \nu^{(k)}\varepsilon_{zz}^{(k)}] \tag{2.47a}$$

$$\sigma_{yy}^{(k)} = \frac{E^{(k)}\nu^{(k)}}{(1+\nu^{(k)})(1-2\nu^{(k)})}(\varepsilon_{xx}^{(k)} + \varepsilon_{zz}^{(k)}) \tag{2.47b}$$

$$\sigma_{xy}^{(k)} = 0. \tag{2.47c}$$

The transverse (through-thickness) stresses are calculated by integrating the equilibrium equations in each sublaminate zone through the thickness coordinate z, neglecting body forces:

$$\sigma_{xx,x}^{(k)} + \sigma_{xz,z}^{(k)} = 0 \tag{2.48}$$

$$\sigma_{xz,x}^{(k)} + \sigma_{zz,z}^{(k)} = 0 \tag{2.49}$$

$$\sigma_{yz,x}^{(k)} + \sigma_{yz,z}^{(k)} = 0. \tag{2.50}$$

First, σ_{xz} is calculated by integrating Equation 2.48, knowing the result of the calculation of σ_{xx} from the constitutive relations (Hooke's law). Then, Equation 2.49 is integrated and solved for the unknown σ_{zz}. The transverse stress expression $\sigma_{yz}^{(k)} = 0$ is the result of the constitutive relations for plane strain, and is presented with the equilibrium equations for completeness.

The following boundary conditions are imposed on the upper and lower surfaces:

$$\sigma_{xz}^{(1)} = 0, \quad \sigma_{zz}^{(1)} = -\frac{q_l}{b} \quad (z = z_1) \tag{2.51}$$

$$\sigma_{xz}^{(3)} = 0, \quad \sigma_{zz}^{(3)} = \frac{q_u}{b} \quad (z = z_4), \tag{2.52}$$

where q_l and q_u are the distributed loads for the lower and upper face sheet, respectively, over the element.

The continuity conditions of displacements and transverse stresses at the sublaminate interfaces are also enforced. These are represented as:

$$u^{(1)} = u^{(2)}, \quad w^{(1)} = w^{(2)}, \quad \sigma_{xz}^{(1)} = \sigma_{xz}^{(2)}, \quad \sigma_{zz}^{(1)} = \sigma_{zz}^{(2)} \quad (z = z_2) \tag{2.53}$$

$$u^{(2)} = u^{(3)}, \quad w^{(2)} = w^{(3)}, \quad \sigma_{xz}^{(2)} = \sigma_{xz}^{(3)}, \quad \sigma_{zz}^{(2)} = \sigma_{zz}^{(3)} \quad (z = z_3). \tag{2.54}$$

For a rigorous, thorough presentation of the layerwise finite element theory, the presentations in [17] and [19] should be consulted.

2.5 Failure Criteria

Once the in-plane and transverse (through-thickness) stresses are calculated, the finite element code computes the average stress over the element length for each stress component, and transforms the average stresses to the principal material coordinate system. These stresses are used to predict failure by the use of existing failure criteria.

Tsai and Wu [27], Hashin [9], and others have developed criteria to predict when failure occurs in an anisotropic material. The failure criteria take a macroscopic approach to the problem, avoiding the complexity of the micromechanics involved and making it possible for one to use relatively simple formulae to predict the occurrence of failure. The Tsai-Wu and Hashin criteria are used in the computational analysis of the sandwich structure. The layerwise finite element method presented herein uses the Tsai-Wu criterion in the core and the Hashin criterion in the face sheets. The Hashin criterion is selected for the face sheets because it is specifically geared to indicate failure modes in a unidirectional composite. Once failure is indicated by one of the failure criteria, the analysis is stopped, and the load that resulted in failure is said to be the failure load for the sandwich beam.

2.5.1 Tsai-Wu Criterion. Tsai and Wu developed a criterion that indicates failure for an anisotropic material that undergoes a three-dimensional state of stress. Failure is said to have occurred when the following condition is met:

$$F \equiv F_i\sigma_i + F_{ij}\sigma_i\sigma_j \geq 1, \tag{2.55}$$

Let X, Y, Z be the lamina normal strengths in tension along the (1, 2, 3) directions; X^*, Y^*, Z^* the lamina normal strengths in compression similarly; and S_{23}, S_{13}, S_{12} the shear strengths in the (23, 13, 12) planes, respectively. Then the F_i and F_{ij} are expressed as follows:

$$F_1 = \frac{1}{X} - \frac{1}{X^*},\ F_2 = \frac{1}{Y} - \frac{1}{Y^*},\ F_3 = \frac{1}{Z} - \frac{1}{Z^*},$$

$$F_{11} = \frac{1}{XX^*},\ F_{22} = \frac{1}{YY^*},\ F_{33} = \frac{1}{ZZ^*},\ F_{44} = \frac{1}{S_{23}^2},\ F_{55} = \frac{1}{S_{13}^2},\ F_{66} = \frac{1}{S_{12}^2},$$

$$F_{12} = F_{21} = -\frac{1}{2}\frac{1}{\sqrt{XX^*YY^*}},\ F_{13} = F_{31} = -\frac{1}{2}\frac{1}{\sqrt{XX^*ZZ^*}},\ F_{23} = F_{32} = -\frac{1}{2}\frac{1}{\sqrt{YY^*ZZ^*}}. \tag{2.56}$$

If failure is indicated, the failure mode is determined by the following expressions [17], where the shorthand notation for coordinate direction from Equation 2.2 is used:

$$H_1 = F_1\sigma_1 + F_{11}\sigma_1^2 \tag{2.57a}$$

$$H_2 = F_2\sigma_2 + F_{22}\sigma_2^2 \tag{2.57b}$$

$$H_3 = F_3\sigma_3^2 \tag{2.57c}$$

$$H_4 = F_{44}\sigma_4^2 \tag{2.57d}$$

$$H_5 = F_{55}\sigma_5^2 \tag{2.57e}$$

$$H_6 = F_{66}\sigma_6^2. \tag{2.57f}$$

The largest H_i is selected as the quantity that determines the dominant failure mode, where:

$$H_1 \rightarrow E_1,\ H_2 \rightarrow E_2,\ H_3 \rightarrow E_3,\ H_4 \rightarrow G_{23},\ H_5 \rightarrow G_{13},\ H_6 \rightarrow G_{12}. \tag{2.58}$$

The stiffness corresponding to the largest H is said to have been reduced as a result of the structural failure by a factor called the stiffness reduction coefficient (SRC). The SRC is an arbitrarily small number (on the order of 10^{-3}), used to reduce the corresponding stiffness well below its original value while keeping it large enough to avoid matrix ill-conditioning.

2.5.2 Hashin Criterion. Hashin provides a criterion that can be used to determine failure mode in a unidirectional composite. Modes of failure predicted by this criterion are fiber failure in tension, fiber failure in compression, matrix failure in tension or compression, and delamination. For this presentation, delamination (separation of plies in the face sheets) is not considered because, as observed in [17], delamination occurs only after the appearance of matrix cracks. Matrix cracking is an indication of the initiation of matrix failure in tension, and this thesis only considers initial failure in the sandwich structure.

Fiber failure in tension in a lamina is predicted for $\sigma_{11} > 0$ when:

$$\frac{\sigma_{11}}{X} + \frac{\sigma_{12} + \sigma_{13}}{S_{12}} \geq 1. \tag{2.59}$$

Fiber failure in compression in a lamina is predicted for $\sigma_{11} < 0$ when:

$$\left(\frac{\sigma_{11}}{X^*}\right)^2 \geq 1. \tag{2.60}$$

Matrix failure in tension is predicted for $\sigma_{22} + \sigma_{33} > 0$ when:

$$\left(\frac{\sigma_{22} + \sigma_{33}}{Y}\right)^2 + \frac{\sigma_{23}^2 - \sigma_{22}\sigma_{33}}{S_{23}^2} + \frac{\sigma_{12}^2 + \sigma_{13}^2}{S_{12}^2} \geq 1. \tag{2.61}$$

Finally, matrix failure in compression is predicted for $\sigma_{22}+\sigma_{33}<0$ when:

$$\frac{\sigma_{22}+\sigma_{33}}{Y^*}\left[\left(\frac{Y^*}{2S_{23}}\right)^2-1\right]+\frac{(\sigma_{22}+\sigma_{33})^2}{4S_{23}^2}+\frac{\sigma_{23}^2-\sigma_{22}\sigma_{33}}{S_{23}^2}+\frac{\sigma_{12}^2+\sigma_{13}^2}{S_{12}^2}\geq 1. \qquad (2.62)$$

In the following chapter, experimental procedure and observations are discussed. Photographs of the specimens are presented to illustrate experimental phenomena. The theories presented above are used later in Chapter IV to compare theoretical predictions to the experimental results.

III. Sandwich Beam Experimental Procedure and Observations

3.1 The Experiments

The objective of the experimental portion of this research is to experimentally demonstrate and characterize failure in the sandwich structure. Similar to previous experimental work in sandwich construction [24], a four-point bend test is performed on a sandwich structure consisting of a carbon foam core and laminated face sheets, keeping both materials and dimensions consistent with the above cited research, but varying face sheet layup in order to observe the potential for failure modes appearing in the face sheets in addition to the core. The only failure mode observed in [24] for the materials and geometry used in this thesis was that of core failure in shear.

The carbon foam was obtained from Touchstone Research Laboratory. It is assumed to have a ligament microstructure, the result of the foam assuming a structure having minimum surface energy during the manufacturing process. The microstructure of the carbon foam is modeled to possess a tetrahedral structure with the foam ligaments oriented approximately 109° with each other. A model of the ligament geometry has been developed by the consideration of the material microstructure as an array of solid tetrahedrons from which spherical voids are removed. These models are depicted in Figures 3.1 and 3.2. The spheres are generated with their centers coincident with the four vertices of each tetrahedron, and the radii of the spherical voids are functions of the porosity of the foam. The porosity of the carbon foam used in this experiment is higher than 80% (its theoretical value is not less than $\sqrt{2}$ for coalescing spheres). The ligaments act as stiffeners, where each ligament can be considered as a beam, and the four ligaments that comprise the tetrahedral microstructure can be considered as a frame or truss structure [25]. See Figure 3.3 for a photograph of the foam microstructure.

This research considers the carbon foam on a macroscopic level. Bulk material properties for the carbon foam are used in the analysis. The carbon foam is anisotropic on a macroscopic scale because when it is formed, the voids in the material are not exactly

Figure 3.1 Three-Dimensional Mesh of Tetrahedral Ligament Microstructure [25]

Figure 3.2 One-Dimensional Mesh of Tetrahedral Ligament Microstructure [25]

spherical. Thus, the voids cause a difference between the strength and stiffness properties in the thickness direction, and those in the plane of the specimen. Furthermore, due to specimen irregularity in the material microstructure, the material properties vary throughout the specimen, making the bulk properties approximate representations of any particular sample.

Carbon foam is selected as a core material because of its high strength-weight and stiffness-weight ratios. Its heat resistance makes it suitable for applications in combustors and similar high-temperature applications. It also has a low coefficient of thermal expansion, which makes it a good candidate for space structures that are exposed to large thermal gradients. It is a good insulator (thermally and mechanically) and can be used in applications requiring energy-absorbing materials [24], since it has the ability to absorb impact energy through crushing (inelastic compression).

The laminated face sheets, consisting of unidirectional long graphite fibers and bismaleimide (BMI) matrix, are provided by the manufacturer in the form of rolled prepreg tape. Prepreg is the short form for preimpregnated fiber-reinforced plastics. Prepregs consist of roving, woven fabric, continuous unidirectional fiber reinforcement sheets, or random chopped-fiber sheets impregnated with a partially cured resin system [1]. The material properties of the prepreg are stated to be equivalent to those of Cytec CYCOM IM7/5250-4 [5].

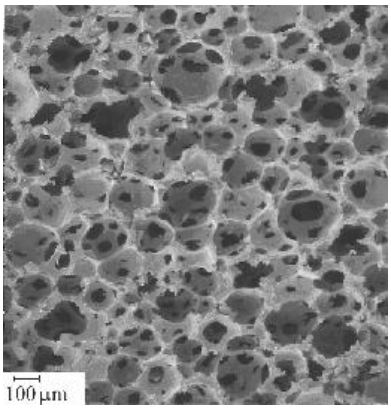

Figure 3.3 Scanning Electron Microscope Image of Carbon Foam [24]

3.1.1 Fabrication of Specimens. The carbon foam core specimens were cut from an approximately 13.9 mm thick sheet, using a diamond wafering saw. Nine beam cores were cut to measure 203.2 mm long by 25.4 mm wide. They were then rinsed and allowed to air dry. After they had dried, the specimens were measured. All dimensions are measured using a caliper, and all masses are measured using a Mettler PE 3600 scale, accurate to 0.01 g. These measurements are presented in Table 3.1.

Table 3.1 Carbon Foam Core Measurements

Specimen	**Width** [mm]	**Length** [mm]	**Thickness** [mm]	**Mass** [g]	**Volume** [cm^3]	**Density** [g/cm^3]
1	25.451	203.20	13.913	33.04	71.952	0.45920
2	25.457	203.20	14.002	34.04	72.430	0.46997
3	25.337	203.20	13.926	33.29	71.694	0.46433
4	25.337	203.20	13.894	34.03	71.531	0.47574
5	25.438	203.20	13.830	34.60	71.489	0.48399
6	25.457	203.20	13.824	33.64	71.510	0.47042
7	25.413	203.20	13.856	33.76	71.549	0.47185
8	25.330	203.20	13.894	33.07	71.513	0.46244
9	25.425	203.20	13.932	33.60	71.978	0.46681
Mean	25.404	203.20	13.897	33.674	71.739	0.46942
Std. Dev.	0.22%	0.00%	0.40%	1.50%	0.45%	1.59%

The laminae were cut from a 304.8 mm wide roll of prepreg tape to measure 304.8 mm by 304.8 mm, in order to prepare two $[0/90/0]_T$ and two $[0/90]_S$ laminates. Symmetric laminate layups were selected so that residual thermal stresses did not cause warping in the laminates as they cured. The laminae were then stacked and prepared for the autoclave. The autoclave, manufactured by Thermal Equipment Corporation, Los Angeles, CA, has a working surface measuring 914.4 mm by 914.4 mm. The laminates were cured at 179 °C for 6 hours under 689 kPa (6.80 atm) of pressure (a vacuum was maintained until the temperature and pressure reached 93 °C and 552 kPa (5.44 atm), respectively), after which they were post-cured at 227 °C for another 6 hours under atmospheric pressure (1.0 atm). The laminates were then allowed to cool to room temperature (about 21 °C) and were visually inspected for damage. No visual evidence of damage due to warping or bubbling was found.

After the laminates cooled, the face of each laminate sheet to be adhered to the carbon foam core was prepared using a media blaster. The 304.8 mm by 304.8 mm sheets were then cut into 203.2 mm long by 25.4 mm wide panels to match the length and width of the foam cores. Six panels were cut from one $[0/90/0]_T$ laminate, and six from one $[0/90]_S$ laminate. The other six panels were cut from the second $[0/90/0]_T$ laminate perpendicular to its 0° fiber direction, so that the resulting panels had a $[90/0/90]_T$ orientation. Face sheet measurements are presented in Table 3.2.

Table 3.2 Laminated Face Sheet Measurements

Specimen	**Width** [mm]	**Length** [mm]	**Thickness** [mm]	**Mass** [g]	**Volume** [cm^3]	**Density** [g/cm^3]
$[90/0/90]_T$ Face Sheets						
1A	25.387	204.79	0.43180	3.25	2.2449	1.4477
1B	25.425	204.79	0.43180	3.11	2.2483	1.3833
1C	25.362	204.79	0.43180	3.23	2.2427	1.4402
1D	25.375	204.79	0.43180	3.26	2.2438	1.4529
1E	25.356	204.79	0.43180	3.27	2.2421	1.4584
1F	25.381	204.79	0.43180	3.16	2.2444	1.4080
$[0/90]_S$ Face Sheets						
2A	25.470	204.79	0.58420	4.36	3.0471	1.4309
2B	25.375	204.79	0.58420	4.35	3.0357	1.4329
2C	25.394	204.79	0.58420	4.35	3.0380	1.4319
2D	25.381	204.79	0.58420	4.38	3.0365	1.4425
2E	25.400	204.79	0.58420	4.31	3.0388	1.4183
2F	25.400	204.79	0.58420	4.31	3.0388	1.4183
$[0/90/0]_T$ Face Sheets						
3A	25.343	204.79	0.43180	3.20	2.2410	1.4279
3B	25.368	204.79	0.43180	3.20	2.2432	1.4265
3C	25.394	204.79	0.43180	3.24	2.2455	1.4429
3D	25.432	204.79	0.43180	3.25	2.2489	1.4452
3E	25.362	204.79	0.43180	3.19	2.2427	1.4224
3F	25.451	204.79	0.43180	3.24	2.2505	1.4397
Mean	25.392	204.79	0.1446/ply	1.08/ply	0.7521/ply	1.4317
Std. Dev.	0.13%	0.00%	0.84%	1.36%	0.75%	1.24%

Values shown in Table 3.3 are average measurements for the laminate and core, and are used as nominal values for computer modeling.

Table 3.3 Measurement Averages for Face Sheet and Core (MKS units)

Mean face sheet mass density	1431.7 kg/m^3
Mean core mass density	469.42 kg/m^3
Mean face sheet ply thickness	0.145×10^{-3} m
Mean core thickness	13.90×10^{-3} m
Mean core width	25.40×10^{-3} m

Once the face sheets were cut to the proper orientation and size, they were adhered to the carbon foam cores using FM73 0.415 kg/m^2 knit carrier adhesive. The adhesive was kept below 0 °C until immediately before use in order to retain its adhesive properties, but was allowed to warm to room temperature before use so it was not brittle. The FM73 adhesive was cut into 203.2 mm by 25.4 mm strips to match the dimensions of the face sheets and cores. Two sheets of adhesive were used for each specimen, one to fasten each face sheet to the top/bottom face of the carbon foam core. As the face sheets and core were held firmly together by hand for approximately 20 seconds, the adhesive warmed slightly and began to hold the face sheets in place, making it easier to handle the specimens. Table 3.4 shows the configuration of each specimen and should be referenced throughout to correlate the specimen number with its constituents.

Table 3.4 Cross-Reference for Face Sheets and Cores

Layup	**Specimen**	**Upper Face Sheet**	**Lower Face Sheet**	**Core**
$[90/0/90]_T$	1	1A	1B	1
	2	1C	1D	2
	3	1E	1F	3
$[0/90]_S$	4	2A	2B	4
	5	2C	2D	5
	6	2E	2F	6
$[0/90/0]_T$	7	3A	3B	7
	8	3C	3D	8
	9	3E	3F	9

The specimens were cured for one hour at 121 °C and 345 kPa (3.40 atm) using a Wabash 267 kN hydraulic press controlled by a Honeywell AV30 dual setpoint TAS5 controller and four Barber-Colman 590 thermostats. As the specimens were heated, the adhesive liquefied and permeated the porous structure of the carbon foam. As the speci-

mens cooled, the adhesive hardened and formed a rigid bond between the face sheets and the cores. In the region where the adhesive permeated the core, it increased the core's density. Figure 3.4 shows the face sheet and core, and the region between them where the adhesive permeated the core. Because the porosity of the carbon foam core was greater than 80% and the open cells of the foam were exposed to the adhesive surface, the adhesive was able to fill the voids as it heated and became less viscous. When the specimen cooled, the porosity on the exterior surfaces of the foam was reduced by the permeated adhesive.

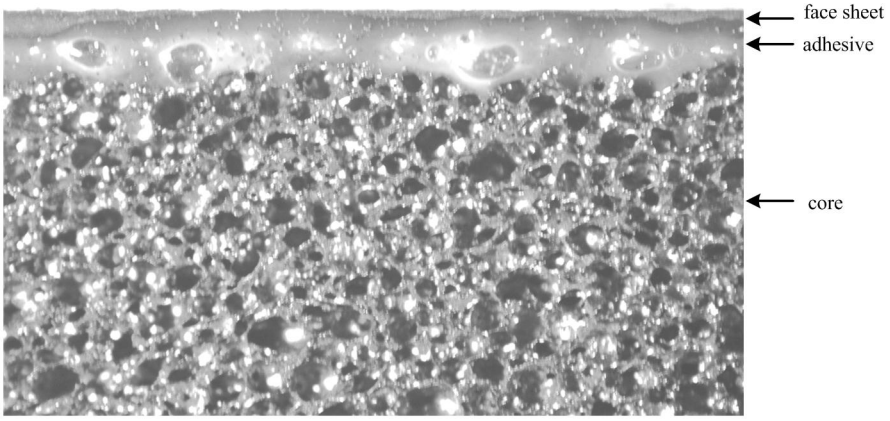

Figure 3.4 Face Sheet, Permeated Adhesive Region, and Core

The prepared specimens were then removed from the press and allowed to cool completely. Before strain gages were applied to the face sheets, the specimens were measured. Measurements for the specimens are recorded in Table 3.5.

The final step in specimen preparation was to place strain gages in the center of each face sheet, resulting in two strain gages for each specimen. All strain gages, strain gage adhesives, and related materials were manufactured by the Micro-Measurements Division, Measurements Group, Inc., Raleigh, NC. The gages used were 125 mill (3.175 μm) CEA-06-125UW-350 precision strain gages, with a gage factor of $2.110 \pm 0.5\%$ and an impedance of $350\,\Omega$ at $24\,^{\circ}$C ($\pm$ 0.3%). They were used to record strain at the midspan

Table 3.5 Specimen Measurements

Specimen	Width [mm]	Length [mm]	Thickness [mm]	Mass [g]
1	25.77	204.79	14.79	43.81
2	25.83	204.79	14.76	44.85
3	25.64	204.79	14.81	44.00
4	25.83	204.79	14.94	47.08
5	25.93	204.79	14.94	47.70
6	25.95	204.79	14.84	46.76
7	25.74	204.79	14.70	44.65
8	25.71	204.79	14.80	43.81
9	25.90	204.79	14.72	44.33

of both the upper and lower face sheets on their exterior surfaces as the sandwich beam specimens were subjected to bending.

The method of applying strain gages to the face sheets as performed by this author was as follows. First, the area on the face sheet where the strain gage was to be attached was treated with 240-grit sandpaper to ensure good adhesion. M-Prep Conditioner A (MCA-1, phosphoric acid) was applied to the surface with a cotton swab to clean the surface, and was removed with another swab. Next, M-Prep Neutralizer 5A (MN5A-1, ammonia water) was applied and removed in the same manner, to neutralize the acid. To assist in gage placement, guide marks were made with a graphite pencil on the face sheet, and cellophane tape (PCT-2A) was placed onto the strain gage. The gage was then lined up and held in place to the face sheet using the cellophane tape, and the tape was gently lifted such that the strain gage remained on the tape and not the face sheet, so that the adhesive could be applied. To improve the adhesion between the strain gage and the face sheet, 200 Catalyst C (isopropyl alcohol) was applied sparingly with a cotton swab to the exposed surface of the gage, then M-Bond 200 Adhesive (cyanoacrylate ester) was spread on the specimen using the wood end of the swab. The cellophane tape was then smoothly pressed onto the face sheet, making sure there were no bubbles in the adhesive and that the adhesive covered the entire surface of the strain gage. It was held firmly in place by hand for one minute, and the tape was gently removed after five additional minutes. This procedure was repeated until eighteen strain gages were placed, one on the upper and

one on the lower surface for each of nine total specimens. Figure 3.5 shows a prepared sandwich specimen.

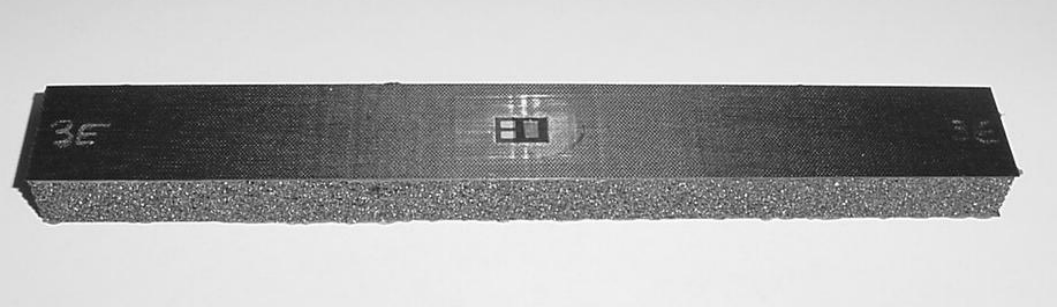

Figure 3.5 Prepared Specimen With Attached Strain Gage (Specimen 9)

3.1.2 Setup and Test Equipment. The sandwich beam specimens were tested with an MTS model 312.31 245 kN hydraulic press controlled by an MTS 458.20 micro-console controller. The controller was set for a load rate of 0.254 mm/min. Each specimen was placed into the test apparatus as shown in Figure 3.6. The cylindrical loading and support pins, made of steel and having a diameter of 6.35 mm, were placed such that the effective beam span (distance between support pins) was 152.4 mm, and the loading span (distance between loading pins) was 76.2 mm. A linear varying displacement transducer (LVDT) was placed at the midspan of the beam and connected to the controller both to record displacement and to use in the feedback control of the press. The strain gages on both surfaces were connected to the controller so strains and displacement could be recorded. Applied load and elapsed time were also recorded.

3.1.3 Experimental Procedure. Specimen 4 was the first tested specimen, as illustrated in Figure 3.6. The specimen was loaded at the rate of 0.254 mm/min until failure. Structural failure was defined to be the displacement at which an increase in the displacement did not correspond to a noticeable increase in the bending load, *i.e.* the displacement at which the structure provided little resistance to further bending. Once this displacement was reached, the controller was disengaged. It was not necessary to be concerned about equipment damage in a displacement-controlled scenario as it would

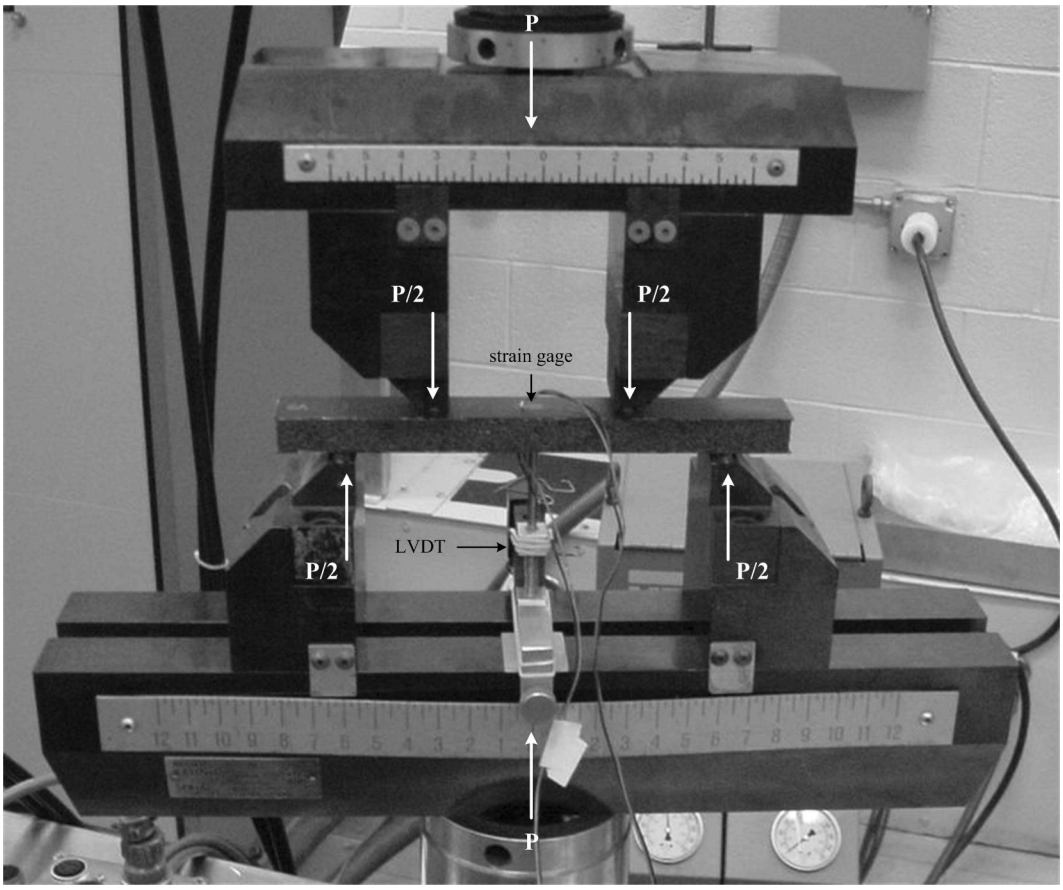

Figure 3.6 Experimental Test Setup (Specimen 4)

have been in a load-controlled scenario, where a dramatic reduction in specimen stiffness due to brittle structural failure would have resulted in a sudden decrease in load followed by the controller commanding a potentially dangerously high increase in displacement in an attempt to keep a constant load rate.

The other specimens were loaded in the same manner until failure, and measurements were taken of elapsed time, total load, midspan displacement, upper surface strain and lower surface strain. Recordings of these measurements were made by a plotter integrated with the MTS controller and by a digital data acquisition system. The digital data was used for the analysis.

3.2 Experiment Observations

Specimen 4, used as a representative sample, exhibited initial failure in the core, as shown in Figure 3.7. The core failed due to shear stress, and the failure immediately propagated through the thickness of the core to the interfaces of the core and face sheets at an angle of 45° from the midsurface. The fact that the structure did not fail symmetrically (*i.e.* for this specimen the core failed on the left side only) is evidence of the variation of material properties throughout the core. One can also surmise from Table 3.1 that since core density measurements vary by approximately 1.6%, the density of the core, and thus its material properties, will also vary slightly throughout the same specimen.

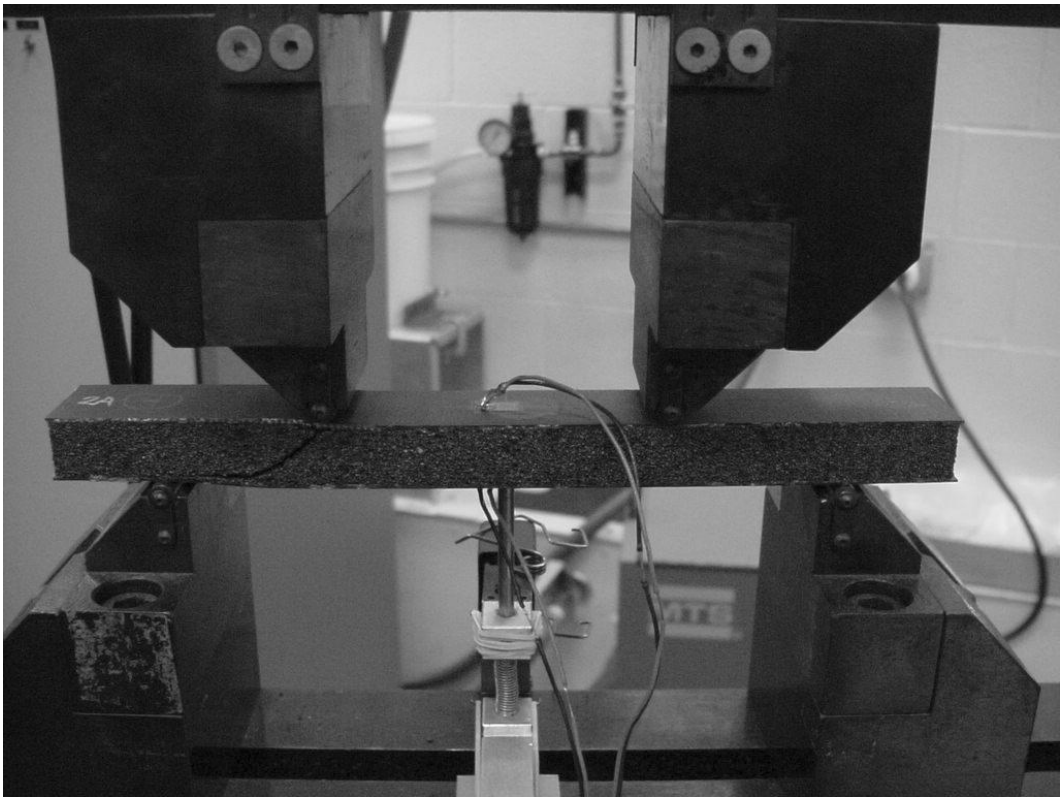

Figure 3.7 Initial Failure Due to Shear Stress in the Core (Specimen 4)

It can also be seen in the figure that the core failure propagated along both the upper and lower interfaces interior to the region where the adhesive permeated the carbon foam.

This happened immediately after the core failed in shear—the failure propagated nearly instantaneously toward the face sheets as they began to peel away from the core.

Figure 3.8 shows a close-up view of a typical core shear failure. Note the ligament microstructure of the core. When the core undergoes shear stress, stress concentrations build up in these ligaments until they are critically stressed. The ligaments break, and brittle failure occurs as the crack rapidly propagates. A secondary shear failure can also be observed in the image, on the left of and almost parallel to the initial shear failure. This secondary failure resulted in a manner similar to the specimen in Figure 3.9.

The crack in the foam appears to propagate from ligament to ligament. This failure mode gives evidence of stress concentrations forming in the ligaments between the voids. The voids cause the foam to be weaker due to these stress concentrations. In a continuous material, the failure would propagate along a 45° line of maximum shear stress through the core, but in the carbon foam the ligaments act as stiffeners and direct the stress distribution and failure. However, observation from experiment photographs indicates a nearly 45° failure propagation through the foam core. This means that the ligaments are not strong enough to direct the stress outside of that failure line on a macroscopic level. However, for one to more accurately consider failure, the failure phenomena due to the ligament microstructure of the foam should be taken into account. The macroscopic failure criteria presented in this study do not have this ability. Also, a careful look at the figure will reveal crushing in the core due to the transverse compressive stress applied by the loading pin. This failure feature can be more easily seen in Figure 3.8 and the additional photos in Appendix B. The compressive failure initiated together with the shear failure at the same load. It can also be seen that the face sheets had pulled away from the carbon foam core. This effect due to peeling stress is discussed in the upcoming text.

Loading was increased after the initial failure, resulting in the secondary failure shown in Figure 3.9. The initial failure weakened the core's ability to carry shear stress in the area of the failure, thus a second crack propagated alongside of the first. The crack varies in direction of propagation because the initial failure changes the material properties

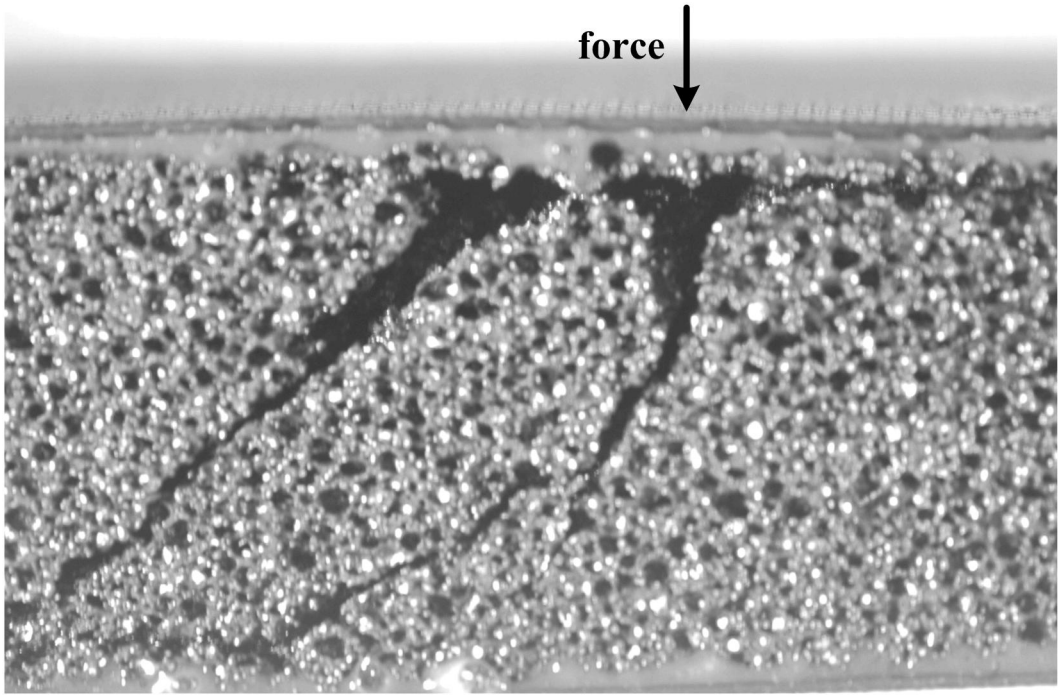

Figure 3.8 Crushing Failure Due to Transverse Compressive Stress (Specimen 7)

of the core such that shear stress may be a maximum at an angle other than 45°, although the second shear stress crack appears to propagate almost parallel to the initial crack. In this region of post-failure, the ligaments are required to carry more stress because of the stiffness reduction that occurred in the failed region. This increase in stress leads to the second crack.

When the specimen was removed from the loading apparatus, the effect of the face sheet pulling away from the core could be readily seen. An example of this is shown in Figure 3.10. As the failure crack propagated along the interface between the face sheet and the core, the absence of support from the core where failure had occurred would have led to the development of a bending moment, causing the face sheet to lift away from the core. Figure 3.11 shows a magnified view of this effect. This effect is known as peeling stress, the result of the bending moment. This bending moment caused the face sheet to develop transverse tensile stress and to pull away from the core.

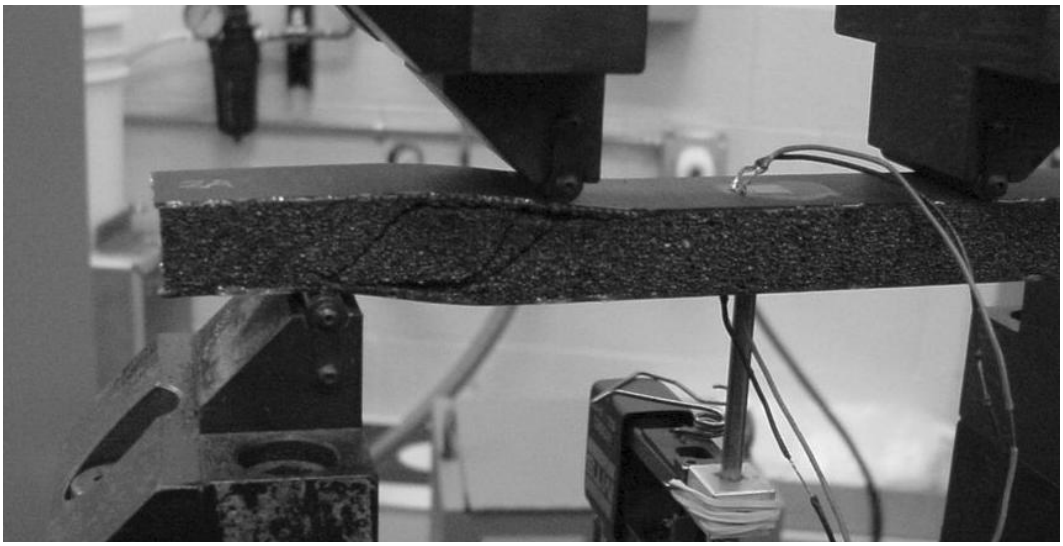

Figure 3.9 Secondary Shear Failure Due to Shear Stress in the Core (Specimen 4)

One can also observe in the figure the effect of the adhesive permeating into the porous carbon foam. Note that debonding did not occur directly between the face sheet and core along the adhesive layer, but rather in the core itself, interior to the permeated region. This is because the adhesive had filled the voids in the porous carbon foam core, which increased the strength of that part of the core by allowing the energy from bending to be transferred from the core to the adhesive.

All eight of the other specimens exhibited failure modes similar to Specimen 4, with the notable exception of Specimen 6. While Specimen 6 responded in failure otherwise similarly to the other specimens, it failed at a markedly lower load than the other two specimens constructed with the same ply layups. This is further evidence of the variation of material properties in the specimens, especially in the core. It is also possible that there existed undetectable damage in the core, which would have reduced its strength. No indication was present to suggest that the structures exhibited failure modes in the face sheet, specifically fiber failure in tension or compression, matrix failure in tension or compression, debonding between ply layers (delamination), or local fiber buckling. Additional photographs in Appendix B show more detailed illustrations of the failed specimens.

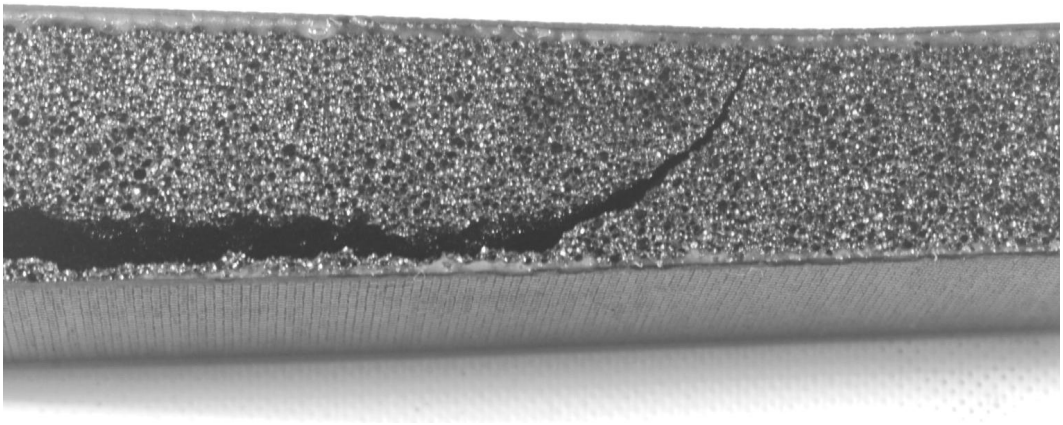

Figure 3.10 Failure Due to Peeling Stress Along Core/Face Sheet Interface (2×) (Specimen 3)

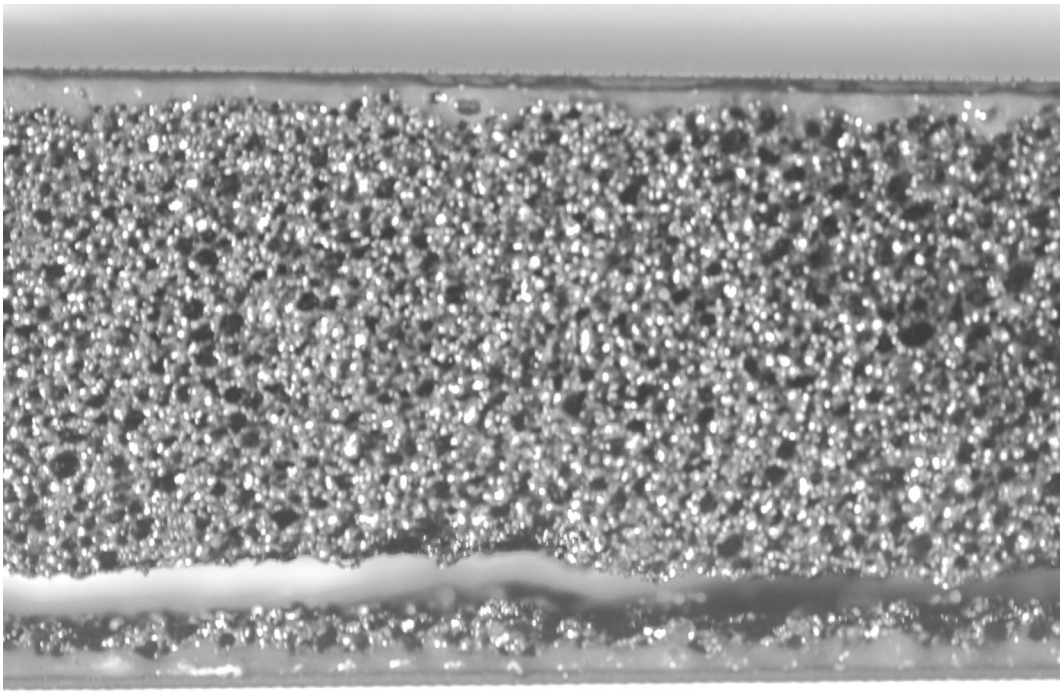

Figure 3.11 Failure Along Core/Face Sheet Interface (5×) (Specimen 9)

In the next chapter, load-displacement and load-strain curves are shown for each sandwich specimen. These results are compared to results from finite element analysis and analytical beam theory.

IV. Finite Element Analysis of Sandwich Beam Construction, and Comparison of Analytical, Computational, and Experimental Results

4.1 Finite Element Model

To computationally evaluate the nodal displacements and element stresses, a finite element model was developed and coded. To use this finite element code, an input file must be created as with any finite element program. The input file includes the solution type, the dimensions and the material properties of the sandwich structure, the nodal and element configuration, the boundary conditions imposed on the structure, and the type of output desired.

4.1.1 Solution Type. For this analysis a linear static solution was performed, applying static concentrated forces in a four-point bend scenario as was physically executed in the experiment. The code was designed to calculate the failure criteria for the core and the face sheet, and to output the results in a separate file. The code also has the ability to generate dynamic solutions given a load distribution with magnitude that is sinusoidal in time; however, time-varying solutions are currently not available when applying concentrated forces to the structure.

The linear solution was performed because the displacements and rotations are not large enough to cause the nonlinear terms to be of any significance. The strain-displacement relationships from Equations 2.37a–2.37f were set up in the finite element code such that each nonlinear term is multiplied by a nonlinear flag bit that is set to 1 for a nonlinear solution and 0 for a linear solution. This procedure effectively removes the nonlinear strain-displacement terms from the linear solution immediately upon their introduction into the code.

4.1.2 Dimensions and Material Properties. For consistency, all inputs to the program are given in SI units. Material properties for the composite laminate and the carbon foam are given in Tables 4.1 and 4.2, respectively.

Material properties for the transversely isotropic composite laminate are obtained from [5]. The italicized quantities G_{23} and S_{23} are not experimentally determined quantities. G_{23} is estimated using the transversely isotropic assumption for the material, Equation 2.8 in Section 2.1. The out-of-plane shear strength S_{23} is obtained from another common graphite/BMI composite [10]. The material properties presented for the carbon foam are from currently available experimental data [24].

Table 4.1 Material Properties of Cytec CYCOM IM7/5250-4 [5]

E_1	162 GPa
E_2	9.7 GPa
$\nu_{12} = \nu_{13}$	0.30
ν_{23}	0.50
$G_{12} = G_{13}$	5.9 GPa
G_{23}	*2.0 GPa*
X	2618 MPa
$Y = Z$	66 MPa
X^*	1620 MPa
$Y^* = Z^*$	248 MPa
$S_{12} = S_{13}$	103 MPa
S_{23}	*77 MPa*

Table 4.2 Material Properties of Touchstone Carbon Foam [24]

E_1	1056 MPa
E_2	1114 MPa
E_3	379 MPa
G	588 MPa
X^*	8.86 MPa
Y^*	10.3 MPa
Z^*	4.38 MPa
S	2.89 MPa

It is important to note that, while compression tests were performed to measure elastic modulus and material strength in all three coordinate directions, the torsion test only gives one material constant for shear modulus. Also, data from tensile tests for this

material are not available. Because of the high porosity of the carbon foam, standard strain measurement techniques are not able to be accurately carried out using strain gages or extensometers. A measurement method such as optical microscopy must be used instead, as discussed in [25]. Since there is currently no tensile test data for this carbon foam, tensile and compressive stiffnesses and strengths are assumed to be equal. This assumption can be removed when more data on the material becomes available.

Also note that the shear strength of the carbon foam material is lower than the compressive strengths. Materials such as Nomex honeycomb, specifically designed for application in sandwich construction, typically have high shear strengths because the core material is expected to undergo primarily shear stress [15]. All of the foams considered for application in sandwich construction in [24] have shear strengths on the order of, or lower than, their compressive strengths. This is a feature inherent to foams, but the foams have the previously discussed advantages, such as excellent thermal management, over other materials. Thus, selection for a core material should not solely be based on shear strength.

The problem geometry was set to match the nominal measurements from the experiment. These values can be found in Table 3.3.

4.1.3 Nodal and Element Configuration. A finite element model was created that consisted of 20 elements and 21 nodes. This model is shown in Figure 4.1. Solution convergence was demonstrated to 2% of midspan vertical displacement upon doubling the number of elements. The cross sections of the finite element nodal point consist of three regions: lower face sheet, core, and upper face sheet. Each ply of the face sheet is considered a nominal layer, and strains are calculated at the midplane of each ply. The core is explicitly divided into nominal layers in the input file, so that stresses and failure can be calculated at various depths within the core. This analysis considered the core as 10 nominal layers.

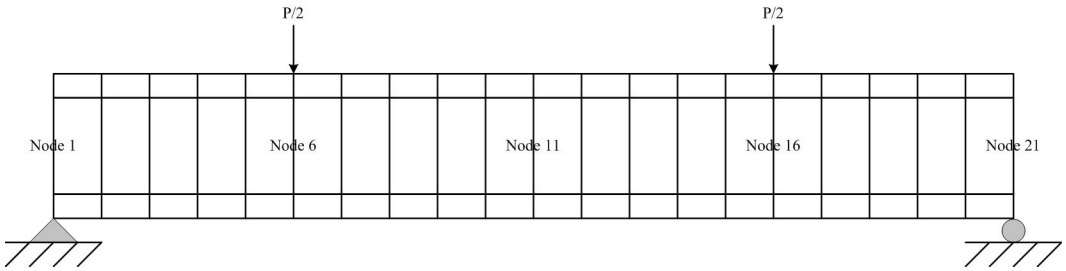

Figure 4.1 Finite Element Model of Sandwich Beam

4.1.4 Boundary Conditions. The boundary conditions for a four-point bending test were imposed on the finite element model. Vertical displacement was constrained at node 1 and node 21, and the point loads were placed on the face sheet upper surface at node 6 and node 16.

4.1.5 Finite Element Program Output. When the program runs, it outputs vertical displacement at a specified node. Node 11 was selected to represent midspan vertical displacement of the sandwich beam. The program also outputs the six three-dimensional stresses at a specified point in the structure. The stresses are calculated through the interpolation functions. For the most part, the stresses are evaluated at the midpoint of each element at the midplane of the ply. The location is based on the optimal coordinates of the interpolation function, which is discussed in detail in [17]. For this analysis, the point for stress output was selected at the center of the core, at a distance halfway between the left support and the left point load. This point approximately represents the location of maximum shear stress in the core. Also, since failure criteria are being calculated, a separate file is created that indicates the presence and mode of failure for each nominal layer in each finite element.

4.2 Comparison of Results

Figures 4.2–4.10 show the load-displacement history for the four-point bending tests performed for this thesis, along with the results for load-displacement slope from the analytical sandwich beam theory, and both the load-displacement slope and failure load

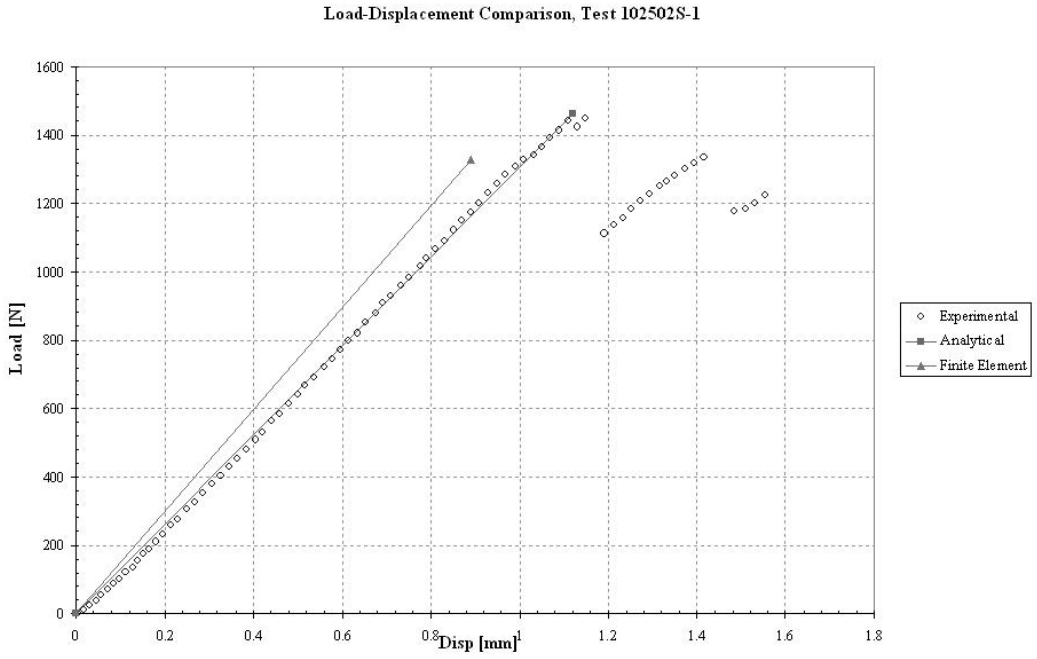

Figure 4.2 Specimen 1 Load-Displacement Results ($[90/0/90]_T$ Layup)

results from the finite element solution. One should note that the analytical beam theory is used here only to obtain the beam stiffness, *i.e.* slope of the load-displacement curves; it does not have the ability to determine failure load.

Initially, the stiffness output from the finite element program was large in comparison with the experimental stiffness and analytical results, up to 30% for some cases. This is believed to be the result of the effect of the cylindrical plate solution assumed by the finite element method. If the narrow beam is modeled as an infinitely wide plate, the result is increased structural stiffness, and a given load will cause a smaller midspan displacement. Therefore, the face sheet elasticity modulus E_1 was reduced by 15% in order see if the effect of cylindrical bending was important. The 15% reduction is an attempt to impose a reduced transverse stiffness, provided by the fibers in the 0° plies of the $[0/90/0]_T$ and the $[0/90]_S$ layups due to the Poisson effect. Thus, it appears that stiffness in the cylindrical bending scenario is quite important, though usually this is not the case. Apparently, the cross-ply orientation characterizes the increased cylindrical bending stiffness.

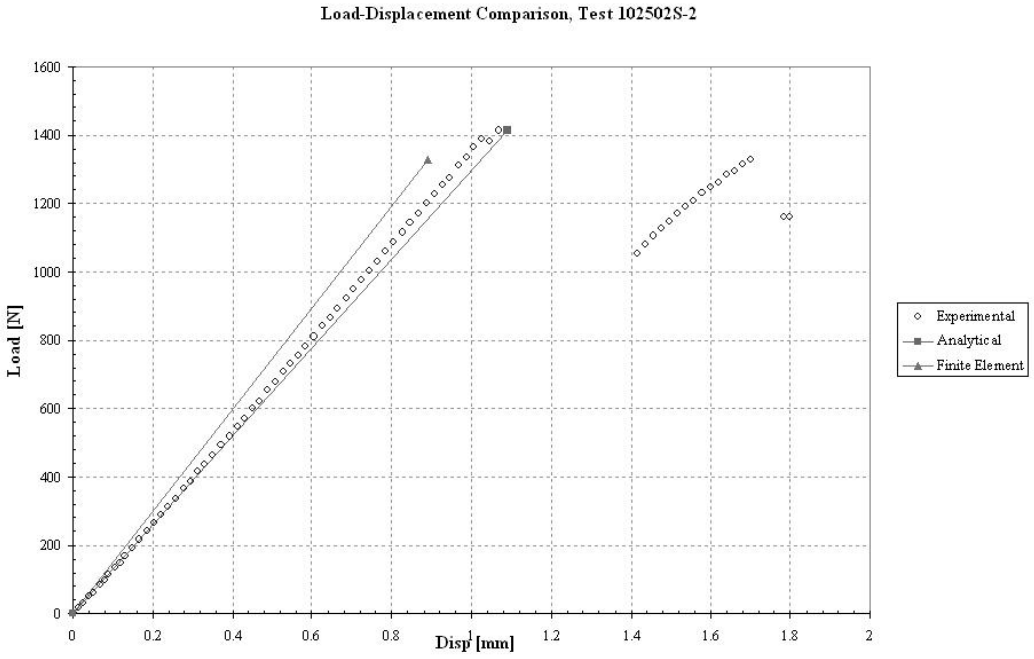

Figure 4.3 Specimen 2 Load-Displacement Results ($[90/0/90]_T$ Layup)

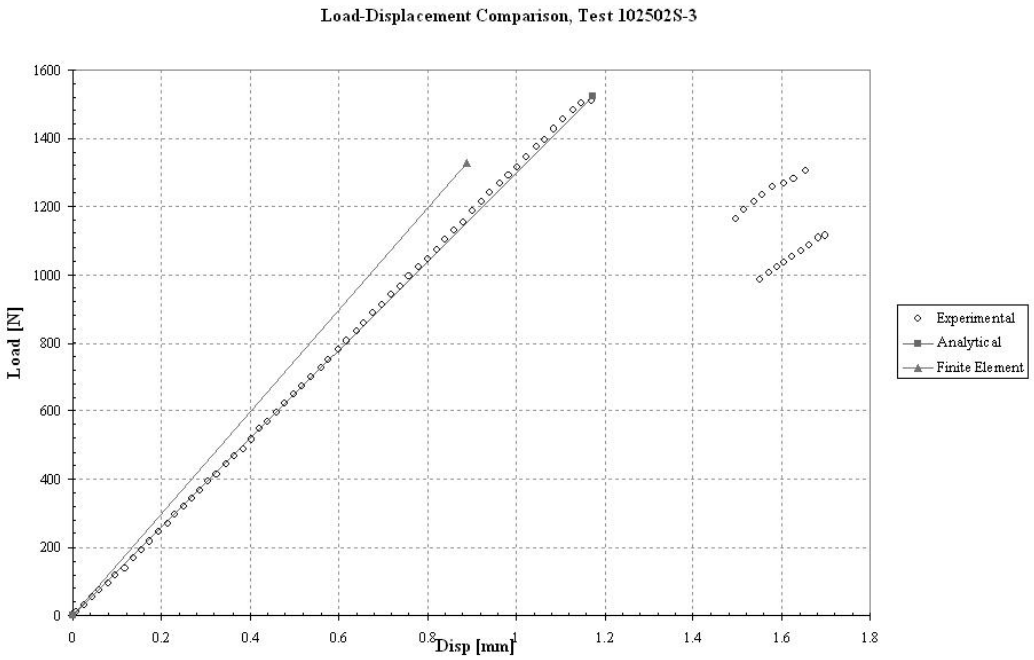

Figure 4.4 Specimen 3 Load-Displacement Results ($[90/0/90]_T$ Layup)

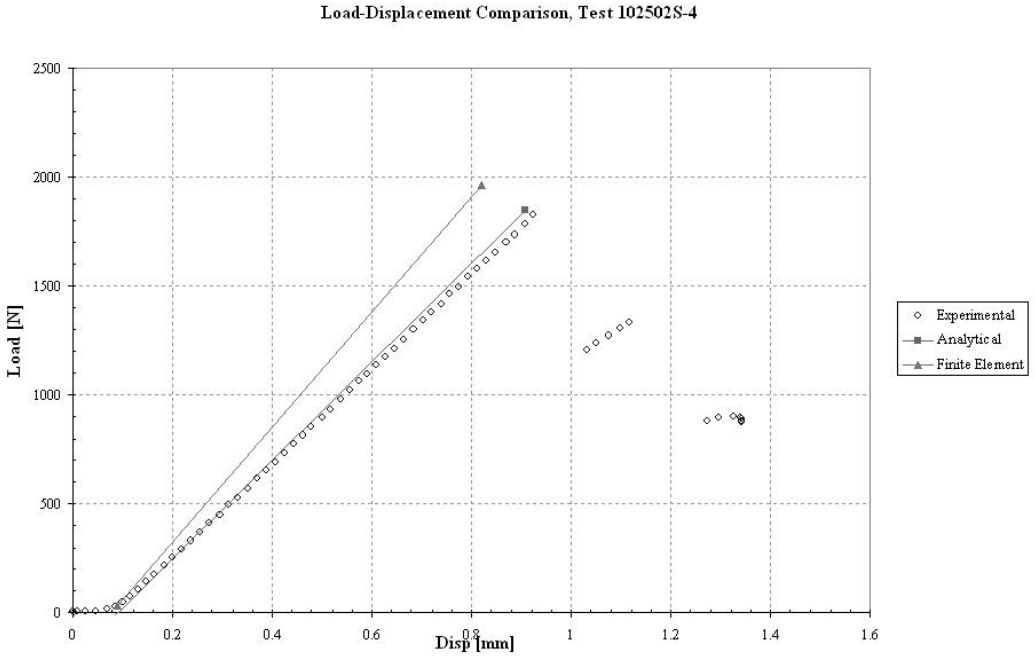

Figure 4.5 Specimen 4 Load-Displacement Results ($[0/90]_S$ Layup)

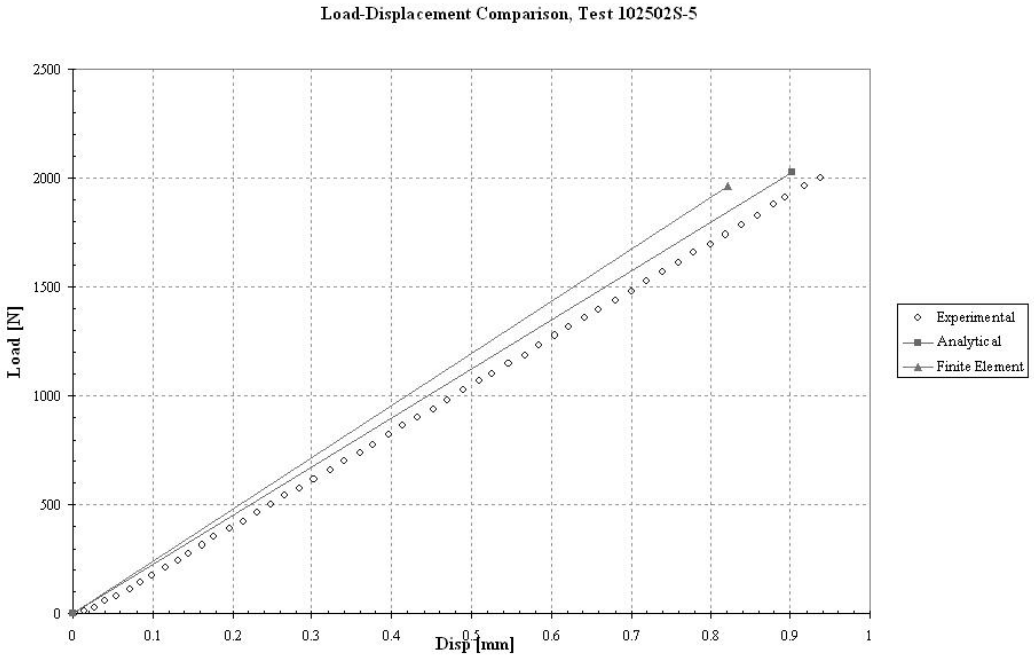

Figure 4.6 Specimen 5 Load-Displacement Results ($[0/90]_S$ Layup)

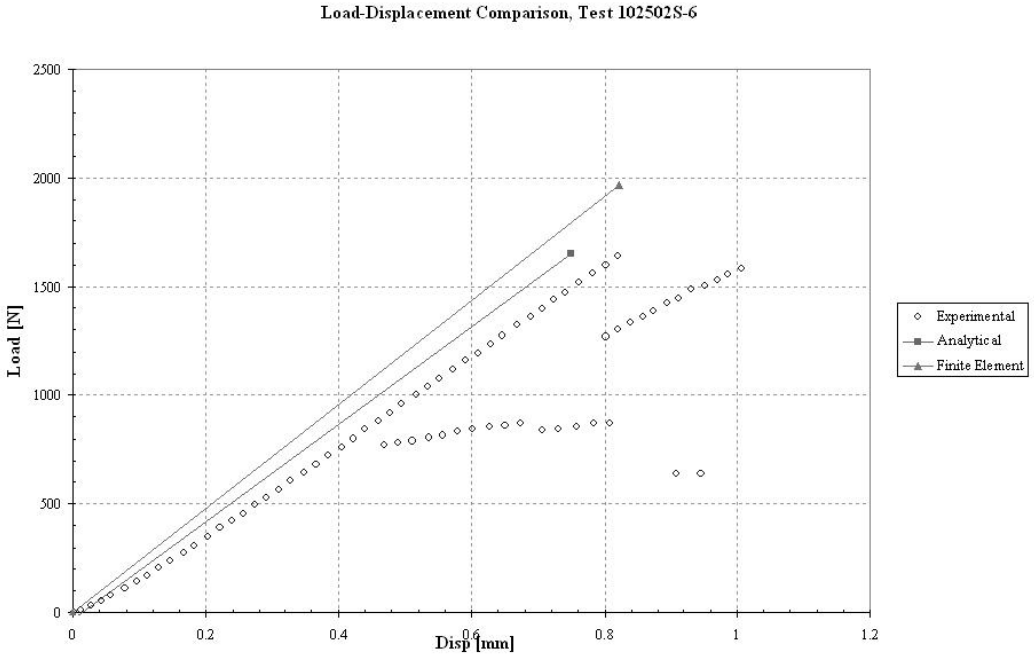

Figure 4.7 Specimen 6 Load-Displacement Results ($[0/90]_S$ Layup)

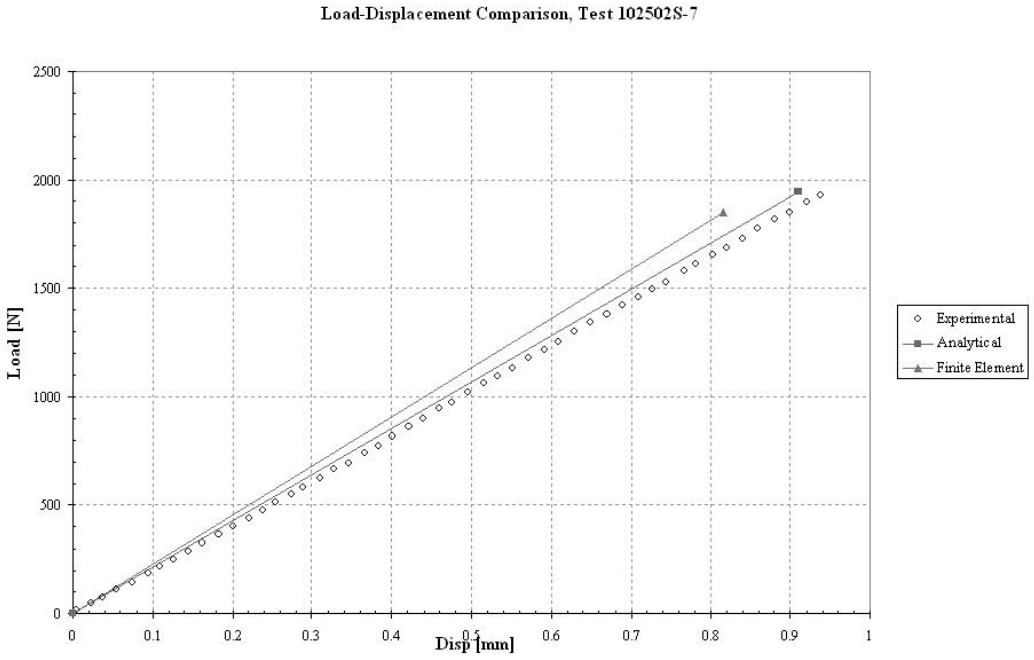

Figure 4.8 Specimen 7 Load-Displacement Results ($[0/90/0]_T$ Layup)

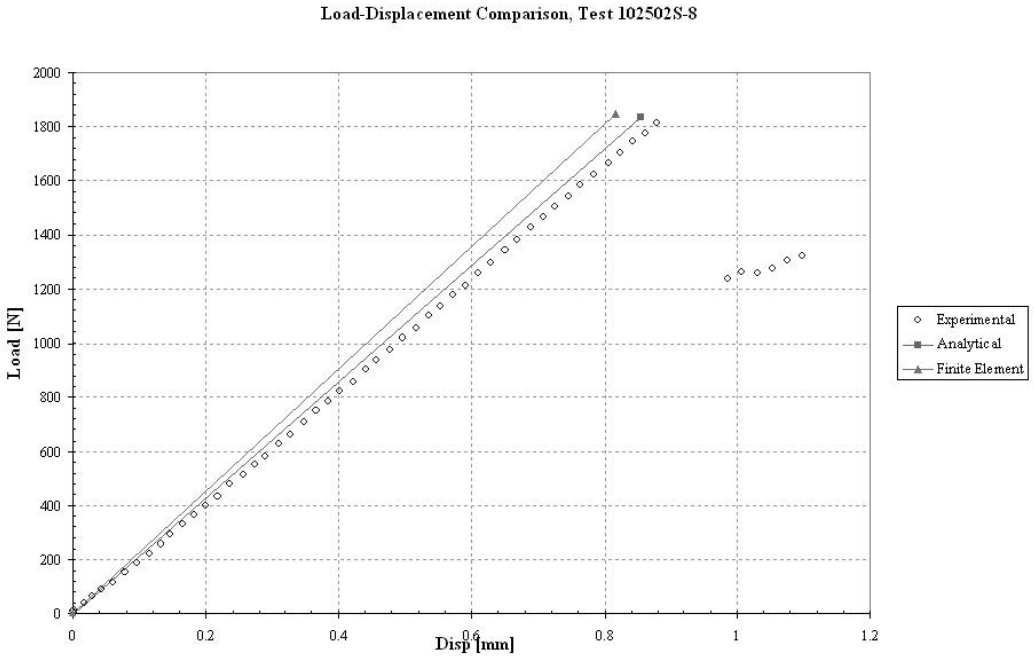

Figure 4.9 Specimen 8 Load-Displacement Results ($[0/90/0]_T$ Layup)

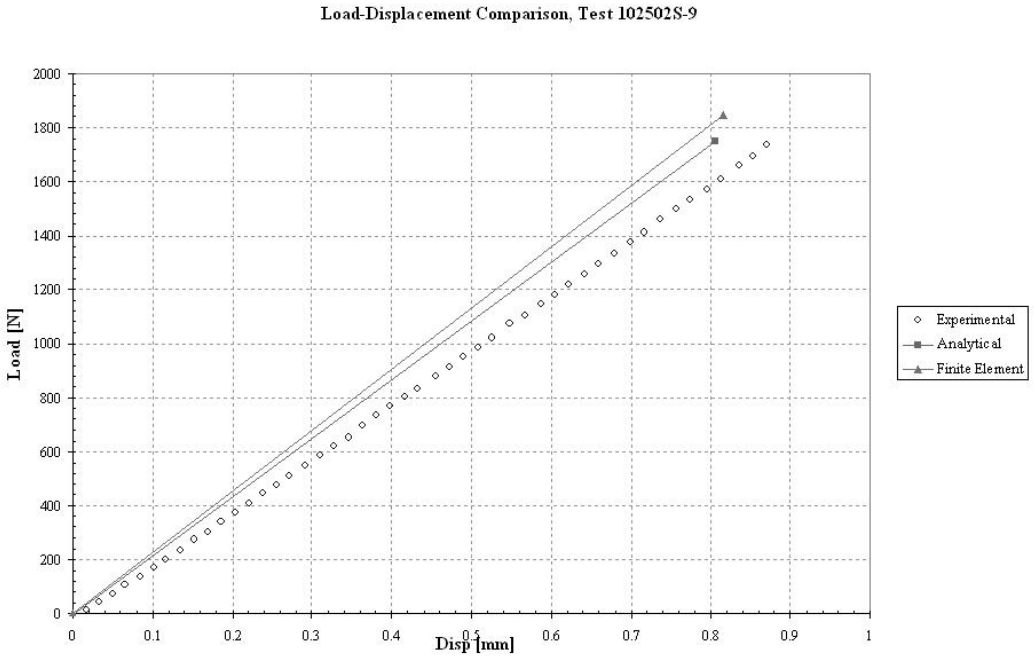

Figure 4.10 Specimen 9 Load-Displacement Results ($[0/90/0]_T$ Layup)

The variation of material properties in the face sheets may also affect the stiffness result. This reduction in stiffness is taken into account in the finite element analysis stiffness results shown in Figures 4.5–4.10. It may be possible to delve further into the program to modify the appropriate algorithms to more accurately consider beam bending.

The failure output from the finite element program indicates that, for all cases considered herein, the core material fails due to shear stress σ_{xz} at a lower load than what is shown in the experiment. The stresses obtained from the finite element solution were used to manually calculate the maximum stress failure criterion in the core, and the same calculation was made using beam theory. Neither of these methods predicted an accurate failure load. For the finite element solution, the maximum load when the shear stress output from the program were manually used to calculate the maximum stress criterion for the $[0/90/0]_{\mathrm{T}}$ layup, for example, was $P = 702.8\,\mathrm{N}$. By way of comparison, for the beam theory solution, the maximum load when shear stress in the core (calculated by Equation 2.35) is equal to the core shear strength S is equal to 2104 N for the three-ply layups ($[0/90/0]_{\mathrm{T}}$ and $[90/0/90]_{\mathrm{T}}$) and 2126 N for the four-ply layup ($[0/90]_{\mathrm{S}}$). For reference, the average experimental failure load was 1456.9 N for the $[90/0/90]_{\mathrm{T}}$ layup, 1821.8 N for the $[0/90]_{\mathrm{S}}$ layup, and 1826.7 N for the $[0/90/0]_{\mathrm{T}}$ layup. The beam theory calculation for maximum shear stress does not take into account the ply layup, only the face sheet thickness (as a parameter in $d = t + c$). Ply layup is clearly an important factor in failure load, however, which can be readily seen by the experimental failure loads shown in the load-displacement charts and in Table 4.3.

This failure analysis leads to the following conclusions. It is possible that the Tsai-Wu failure criterion is not appropriate for the core material used in this study. Since Tsai-Wu makes no consideration of the material microstructure, there may be another criterion that could be developed to take this into account. It is also possible that the test methods used to determine stiffnesses and strengths for the core are actually measuring the microstructural response of the carbon foam as a structure of interconnected trusses,

rather than its material response. Perhaps there is a different test method that can be used other than the test methods typically used for homogeneous materials.

To verify the results of the finite element solution, the stresses and midspan displacements for an isotropic beam were compared to the results from beam theory, with a difference in displacement of 0.4% and difference in shear stress of 11%. One should note, however, that beam theory is not geared to the consideration of through-thickness stresses. Extensive comparisons for sandwich plates under uniform loading appear in [17]. When finite element analysis results were compared to exact solutions from elasticity theory, it was found that the errors in the stress and displacement fields were less than 0.50% for most geometries. These comparisons were carried out both for homogeneous isotropic sandwich plates, and for sandwich plates having isotropic face sheets approximately 10^3 times stiffer than the isotropic core.

Another reason for the variance in results is the variance in material properties in the core specimens. Material properties for the core vary even in the same specimen, as was seen by the different crack locations in the experiment and variation in core densities.

To investigate the applicability of the Tsai-Wu failure criterion, a phenomenological approach to failure analysis was taken. Since the Tsai-Wu criterion did not compare favorably to the experimental data, another criterion was established in which the shear failure calculated by the program was suppressed and not allowed to set the damage flag indicating the material had failed. The load was then increased until another failure mode was indicated. The failure mode that was found was peeling failure due to tensile stress σ_{zz} in the face sheet. This failure is also seen in the photographs of the failed specimens (*e.g.* Figure 3.11) that show the face sheet pulling away from the core region, and is described in that section. It was experimentally shown that the adhesive between the face sheet and the core remains intact through failure, so when the face sheet pulls away from the core, the adhesive and the part of the core permeated with the adhesive both pull away from the core along with the face sheet. This failure phenomenon occurs nearly immediately

after the core fails due to shear stress. Thus, the phenomenological failure methodology appropriately describes what occurred with the specimens in the laboratory.

Using the foregoing methodology for calculating onset of failure, the critical load predicted by the finite element program was compared to that obtained by experiment. Beam stiffnesses were also compared between experiment, sandwich beam theory, and finite element analysis. The results appear in Table 4.3.

Table 4.3 Experimental, Analytical, and Finite Element Load-Displacement and Failure Results

Load/Displacement [N/mm]						**Ultimate Load** [N]		
Specimen	Exp.	FEA	Error (%)	Analytical	Error (%)	Exp.	FEA	Error (%)
1	1336.3	1491.1	11.58	1302.3	2.55	1447.9	1328.0	-8.28
2	1381.4	1491.1	7.94	1298.9	5.97	1414.1	1328.0	-6.09
3	1327.2	1491.1	12.35	1297.8	2.22	1508.8	1328.0	-11.99
4	2185.2	2390.4	9.39	2256.6	3.27	1823.3	1964.4	7.74
5	2152.9	2390.4	11.03	2246.6	4.35	2001.7	1964.4	-1.86
6	2051.0	2390.4	16.55	2246.9	9.55	1640.5	1964.4	19.74
7	2076.7	2264.8	9.06	2141.1	3.10	1929.6	1847.6	-4.25
8	2070.5	2264.8	9.38	2149.0	3.79	1813.5	1847.6	1.88
9	2002.2	2264.8	13.11	2175.6	8.66	1737.0	1847.6	6.37
Mean			11.16%		4.83%			7.58%
Std. Dev.			2.63%		2.67%			5.57%

As mentioned in Chapter III, Specimen 6 failed at a lower load than specimens 4 and 5. The author wishes to highlight that difference in Table 4.3 and restate that this is evidence of the variation in material properties of the constituents of the sandwich structure. There is also a noticeable range of stiffness and strength data for the other specimens. These variations may also be the result of variations in testing parameters (*e.g.* sensor placement) across the experimental trials.

Figures 4.11–4.19 show the load-strain curves for the nine experiments performed. The analytical formula that correlates load to strain is found in Equation 2.34. Bottom face sheet strain is displayed here; the strain on the top face sheet was opposite in sign of, and similar in magnitude to, the bottom face sheet strain, as there was no in-plane failure in any of the face sheet plies.

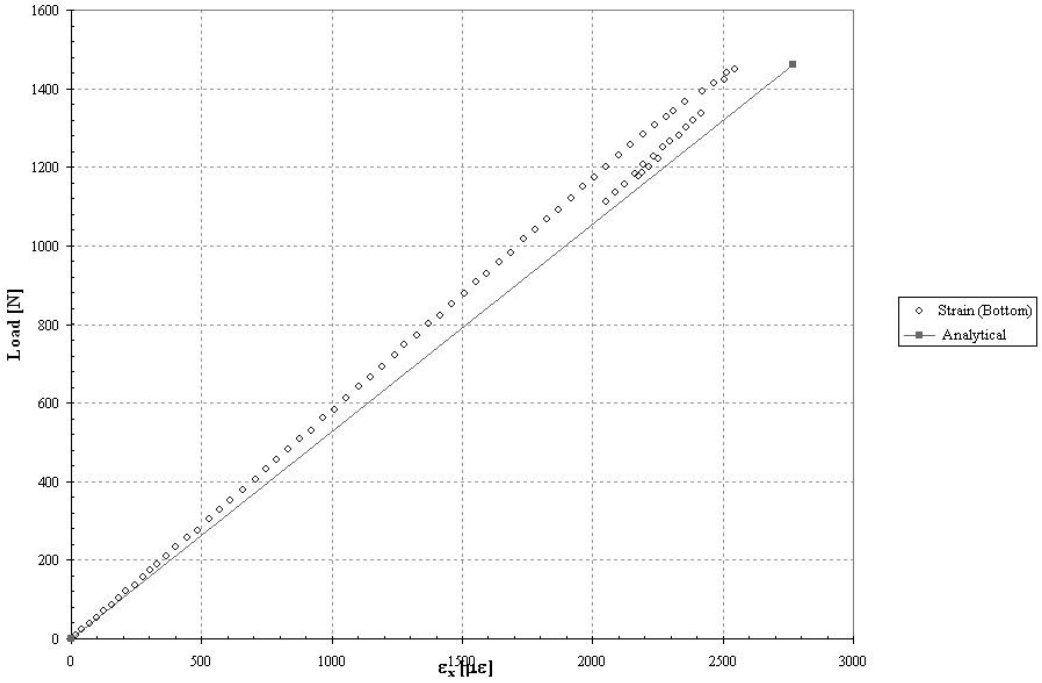

Figure 4.11 Specimen 1 Load-Strain Results ($[90/0/90]_T$ Layup)

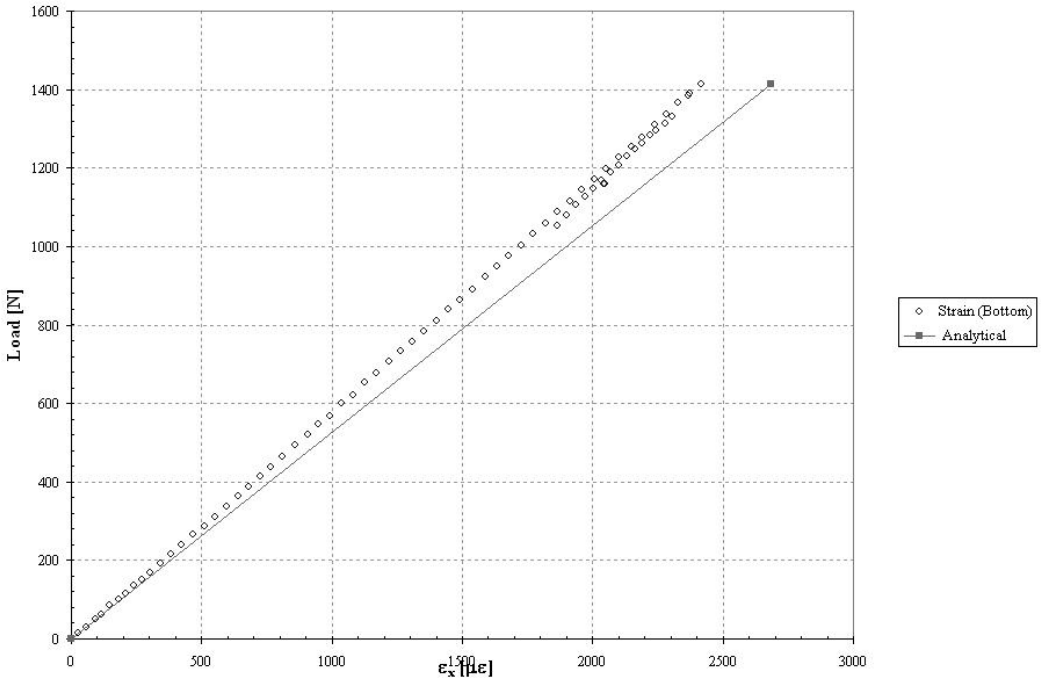

Figure 4.12 Specimen 2 Load-Strain Results ($[90/0/90]_T$ Layup)

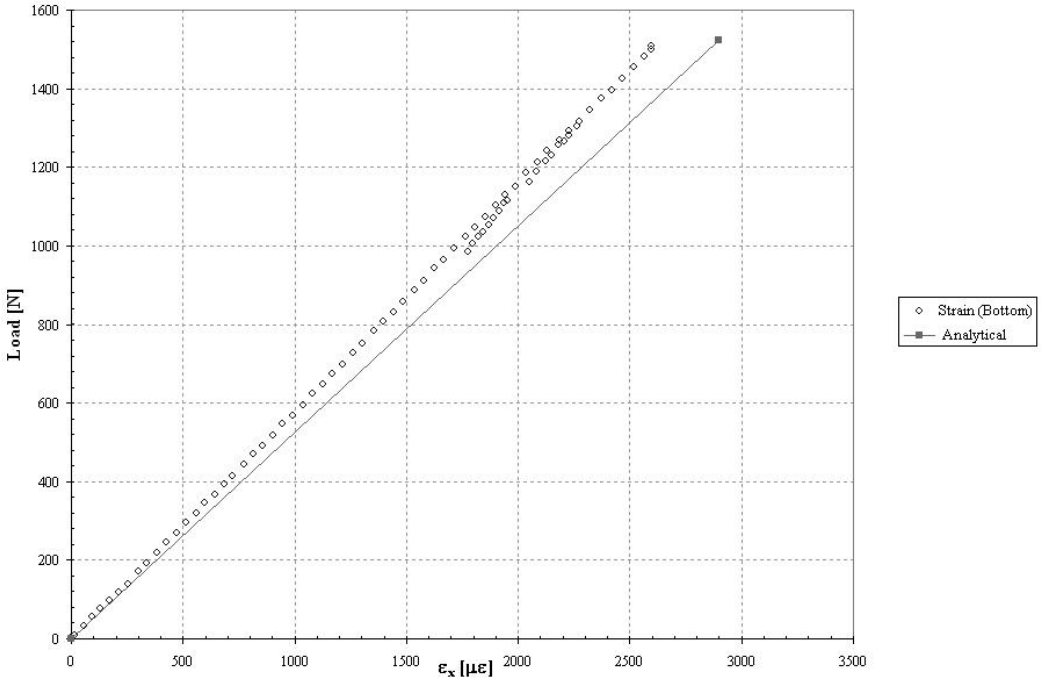

Figure 4.13 Specimen 3 Load-Strain Results ($[90/0/90]_T$ Layup)

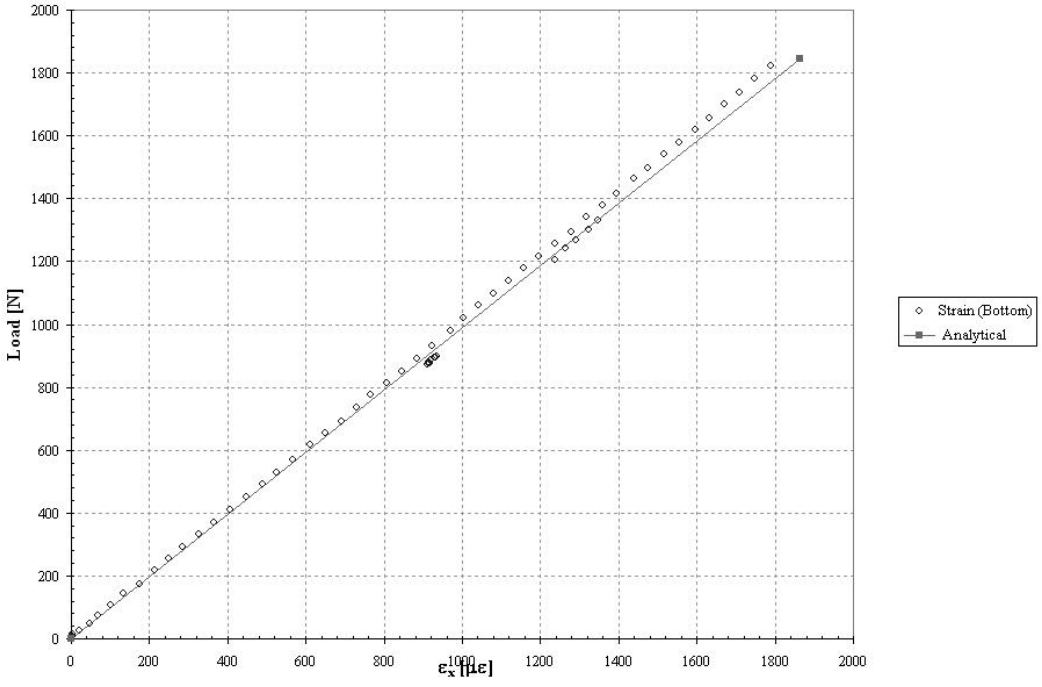

Figure 4.14 Specimen 4 Load-Strain Results ($[0/90]_S$ Layup)

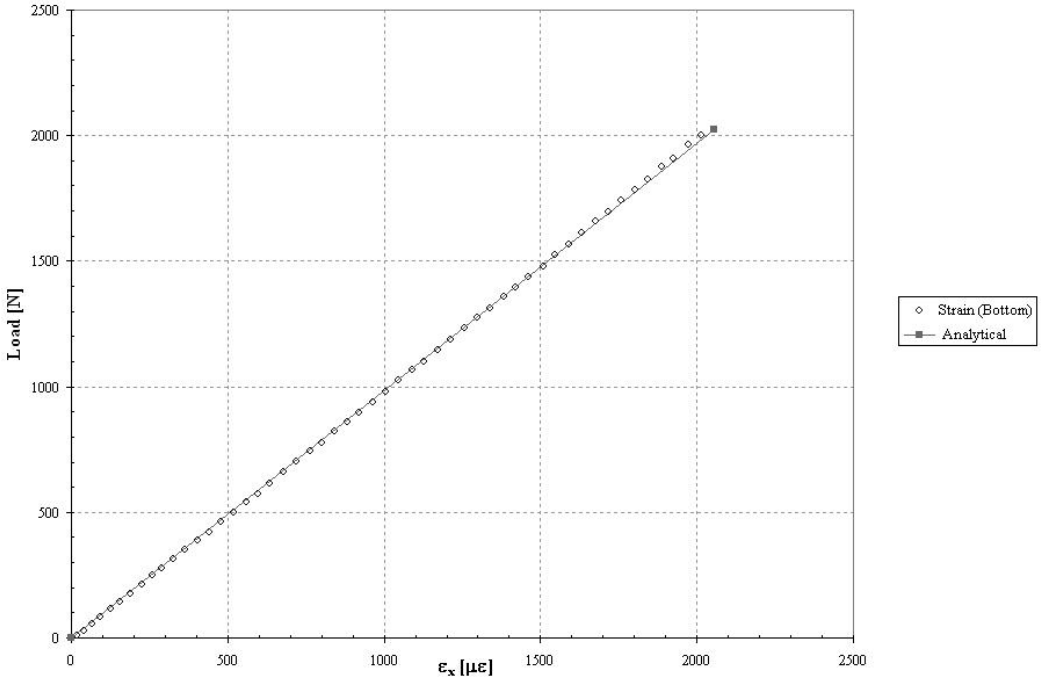

Figure 4.15 Specimen 5 Load-Strain Results ($[0/90]_S$ Layup)

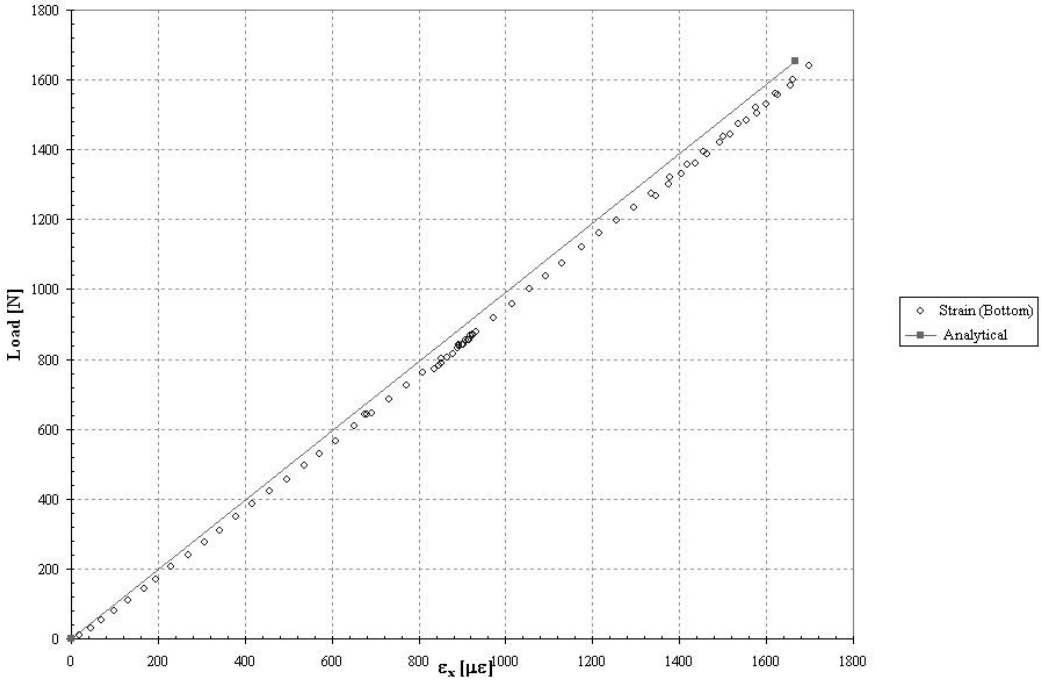

Figure 4.16 Specimen 6 Load-Strain Results ($[0/90]_S$ Layup)

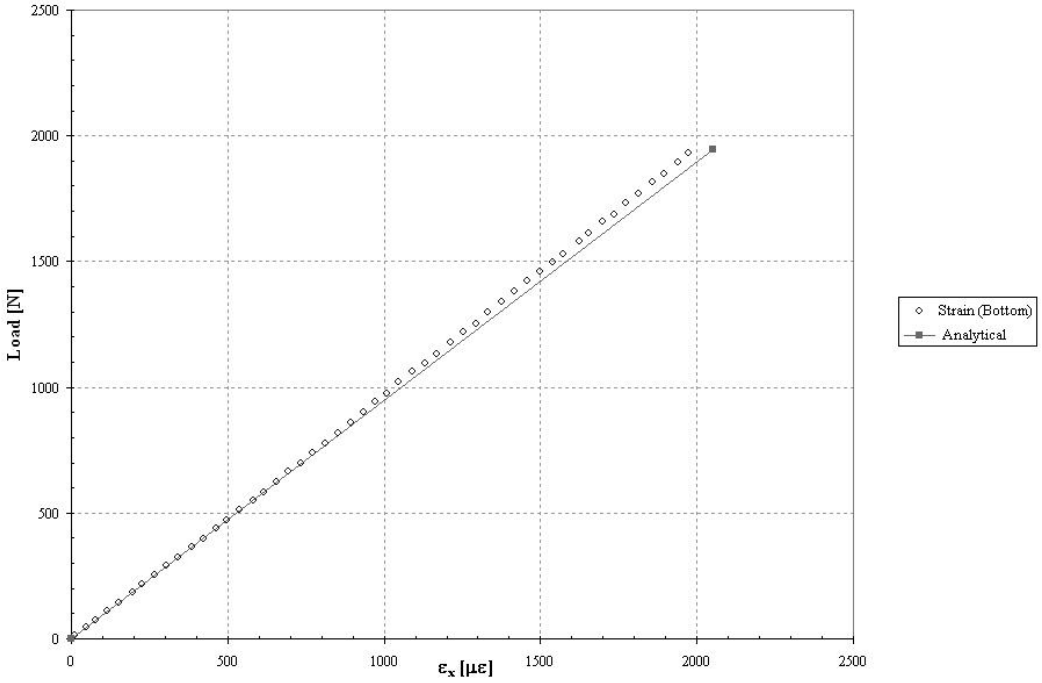

Figure 4.17 Specimen 7 Load-Strain Results ($[0/90/0]_T$ Layup)

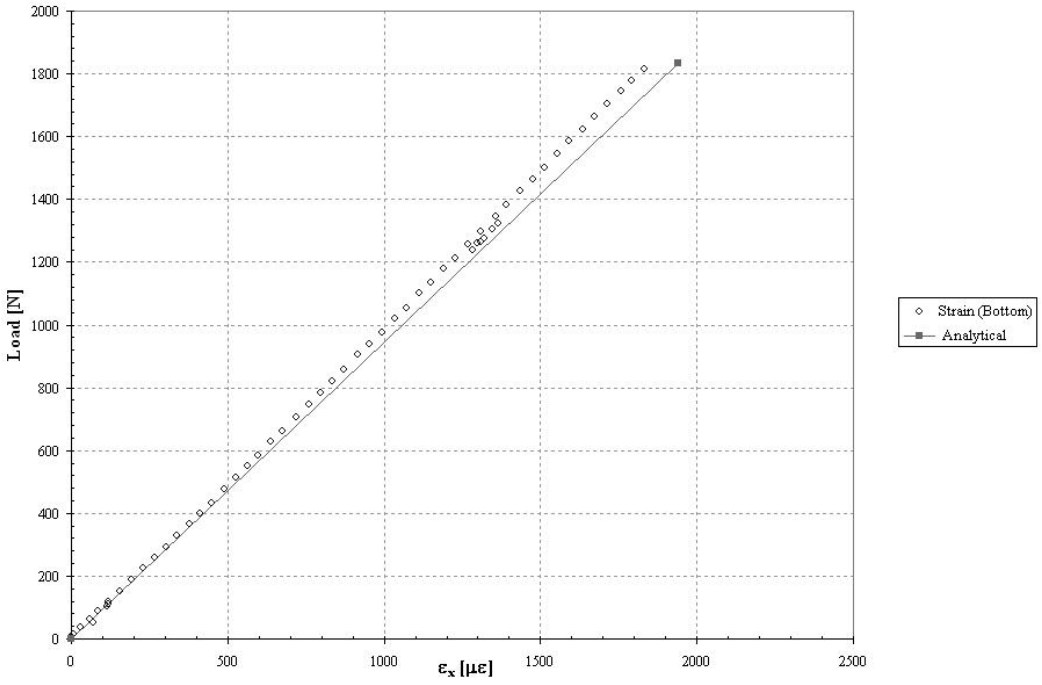

Figure 4.18 Specimen 8 Load-Strain Results ($[0/90/0]_T$ Layup)

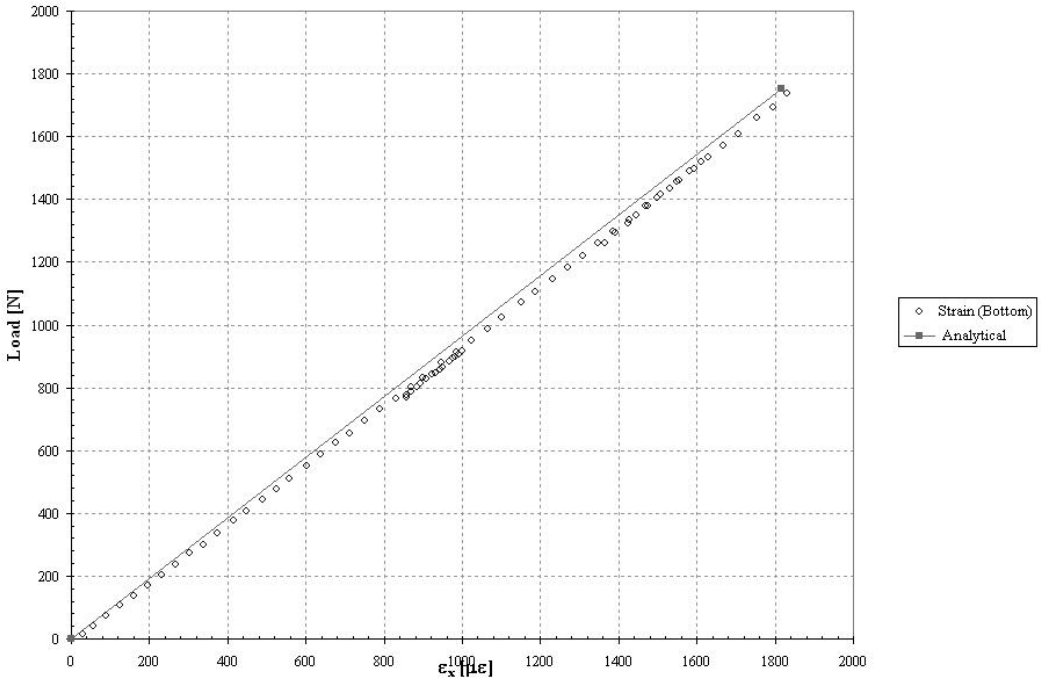

Figure 4.19 Specimen 9 Load-Strain Results ($[0/90/0]_T$ Layup)

Table 4.4 shows the experimental load-strain slope, and the error between the analytical prediction and the experimental outcome.

As briefly discussed above, the Tsai-Wu criterion [27] is applicable to anisotropic materials but does not consider the three-dimensional microstructure of a material. The applicability of the criterion is based on the fact that a continuum is being considered, whereas the material in this study may be more accurately considered as a structure requiring a three-dimensional model. Tsai-Wu does not consider three-dimensional material features, and the results from this study suggest that there may be a more appropriate criterion for the carbon foam.

A finite element model based on the tetrahedral structural model of the ligaments is being developed, as presented in [25]. The three-dimensional and one-dimensional meshes for the tetrahedral structural models are shown in Figures 3.1 and 3.2. It was found by the authors in the above cited work that the solution time for the three-dimensional mesh

Table 4.4 Comparison of Experimental and Analytical Load-Strain Slopes

Specimen	**Experimental** [kN]	**Analytical** [kN]	**Error (%)**
1	580	527	9.13
2	592	527	11.06
3	584	525	10.15
4	1029	990	3.82
5	1000	985	1.50
6	971	991	2.06
7	990	949	4.14
8	1000	946	5.40
9	962	964	0.21
Mean			5.27%
Std. Dev.			3.97%

rapidly increases as the selection of the input parameters (size, orientation, etc.) increases to an impractical value. The authors suggest using a statistical method along with the one-dimensional model to account for variance in cell size and orientation. However, the applicability of such a small-scale model to a relatively large sandwich structure may be limited.

To further investigate material failure using the finite element method presented here, another failure criterion may be considered for the core region to see if the failure result is more aligned with the results of the experiment. It would be beneficial to apply or develop a failure criterion that considers failure based on the porosity of the foam and the shear flow that is produced in the ligaments.

V. Conclusions and Future Work

5.1 Conclusions

Upon completion of the experiments and consideration of the results, including the comparisons between experimental results and theoretical calculations, a summary is presented as follows to report the primary findings of the research.

- This research demonstrated the potential for the layerwise finite element model to be used in the prediction of onset and location of failure. The finite element solution predicts secondary failure at an average 7.58% difference from experiment, with a standard deviation of 5.57%, and stiffness of an average 11.16% difference from experiment, with a standard deviation of 2.63%. The distribution of errors for failure was approximately symmetric about zero, whereas the finite element solutions for beam stiffness were consistently stiffer than the experimental measurements.
- By way of comparison, the analytical sandwich beam theory predicts stiffness of an average 4.83% higher than experiment, with a standard deviation of 2.67%. The closer result from beam theory is an indication of the increased bending stiffness of the plate model developed in the layerwise finite element method.
- Analytical load-strain calculations compare to measured load-strain slope by an average of 5.27% difference from experiment, with a standard deviation of 3.97%.
- The Tsai-Wu criterion does not fit the experimental data for shear failure in the core. The core has a complex three-dimensional ligament truss microstructure. The application of shear stress to the sandwich beam structure causes shear flow to develop in the ligaments; quadratic failure criteria such as Tsai-Wu do not consider this phenomenon.
- Core failure in shear is apparently associated more with the micromechanics of the problem than with the core's aggregate properties. Valid results for failure were not

achieved simply by considering the core as a homogeneous continuum in both the finite element method and the analytical technique.

- It has been found that the peeling stress phenomenon plays an important role in structural failure. A finite element method used to analyze sandwich structures should include the peeling stress component. By using a phenomenological approach to failure analysis, the finite element solution correctly describes this failure mode.
- The carbon foam core has nonhomogeneous properties. Its strength varies throughout each specimen, and from specimen to specimen. Therefore, its failure response also varies depending on the specimen.
- Face sheet stiffness is important in determining the failure load for the sandwich beams. The average failure load for the $[90/0/90]_{\mathrm{T}}$ layup was 1457 N, compared with an average failure load of 1827 N for the $[0/90/0]_{\mathrm{T}}$ layup. On the other hand, the analytical sandwich beam theory predicts equal core shear stress for sandwich beams having the same geometry.
- Penetration of adhesive into the porous foam core affects the experimental failure response of the sandwich beams. The adhesive strengthens the exterior core surface, reinforcing it by filling in the voids and allowing energy from bending to transfer to the cured adhesive. When the structure fails, the face sheet peels away from the core with the adhesive layer intact.

5.2 Future Work

This thesis investigated face sheets of varying layups and thicknesses in an attempt to observe some indication of failure in the face sheets. No failure modes were observed in the face sheets. Dimensions and materials used in the construction of the sandwich beam can be changed to see where the face sheets begin to support the failure in the core by undergoing ply-level failure or delamination. Also, since the core material used in this study is relatively new, additional experiments can be performed to better determine

its material properties, especially its strength and stiffness in shear, as these attributes are critical to the failure response. Dynamic experiments could also be performed and compared to dynamic finite element solutions. It also may be possible to investigate the modification of appropriate algorithms in the finite element program to more accurately consider beam bending.

The author suggests the consideration or development of a different failure criterion for the core. The failure criterion should consider the microstructure of the carbon foam and the interaction in a sandwich structure between the core and the face sheets. It has been found that the Tsai-Wu criterion may not give a good indication of the onset and mode of failure for the carbon foam, so it is possible that another failure criterion is better suited for this material, as demonstrated by the phenomenological approach taken in this study. The face sheets also play a role in the failure of the sandwich beams by affecting the load at which the core fails in shear and the face sheets begin to peel away from the core. This study of failure and subsequent modification of the Tsai-Wu criterion has the potential to lead into the development of a new failure criterion for porous materials.

Appendix A. Finite Element Code Input Instructions, Sample Input File

A.1 Finite Element Code Input Instructions

The following instructions were provided for running the layerwise finite element code as developed in [17] and [19]. A dagger (†) indicates entries that were not needed for the analysis performed in this thesis.

Units – SI units.

Coordinate System – A right-handed orthogonal Cartesian coordinate system is used. The global system of coordinates is chosen for the plates such that the x-axis lies in the direction of the span of the plate.

Data Entry – The concentrated forces are entered only for static analysis. In dynamic analysis, the number of concentrated forces (**NumConcentLoads** in Card 12) must be set equal to zero.

CARD 1:

AnalysisType – Defines the type of analysis to be carried out.

1 – Nonlinear time history with damping and damage progression.

2 – Nonlinear time history with damping and without damage progression.

3 – Linear time history with damping and damage progression.

4 – Linear time history with damping and without damage progression.

5 – Linear static analysis.

6 – Eigenvalue analysis.

7 – Nonlinear static analysis.

8 – Linear static analysis with damage progression.

9 – Nonlinear static analysis with damage progression.

NumFacePlies – Number of plies in each face sheet.

FaceMassDensity – Mass density of face sheet.

FaceThickness – Thickness of one ply of the face sheets (all plies are assumed to have equal thickness).

IncludeCPT – Include classical plate theory.

0 – Assumed transverse strains are not set equal to zero.

1 – Assumed transverse strains are set equal to zero.

CARD 2:

E1Face, E2Face, E3Face, G12Face, G13Face, G23Face, ENu12Face, ENu13Face, ENu23Face – Elastic constants for the face sheet.

CARD 3:

XT, XC, YT, YC, ZT, ZC, S12, S13, S23 – Material strength properties for the face sheets.

TOPAngle(I), (I=1,NumFacePlies) – Ply angles for top face sheet (bottom to top).

BOTAngle(I), (I=1,NumFacePlies) – Ply angles for bottom face sheet (bottom to top).

CARD 4:

NumCorePlies – Number of arbitrary plies in the core.

CoreMassDensity – Mass density of the core.

CoreThickness – Total thickness of the core.

CARD 5:

E1Core, E2Core, E3Core, G12Core, G13Core, G23Core, ENu12Core, ENu13Core, ENu23Core – Elastic constants for the core.

CARD 6:

XTCore, XCCore, YTCore, YCCore, ZTCore, ZCCore, S12Core, S13Core, S23Core – Material strength properties for the core.

CARD 7:

NEqualLength – 1 for equal length FE mesh. 0 for unequal length FE mesh.

PanelLength – Length of panel.

PanelWidth – Width of panel.

NumElements – Number of finite elements.

CARD 8†: – (Note: Skip this card if NEqualLength=1)

X(I), (I=1,NumElements+1) – x-coordinates of nodes for unequal FE mesh.

CARD 9:

RigidBodyMass – Mass of rigid body resting on face.

X1 – Location of beginning of rigid body.

X2 – Location of end of rigid body.

CARD 10:

Fzero – Amplitude of external sinusoidal force on the upper surface per unit area

fPeriod – Period of external force.

X2 – Initial phase of force.

CARD 11:

Src – Stiffness reduction coefficient, src=0.001

SRC – Stiffness reduction coefficient, SRC=0.01

S – Scale for damage function in “delamination” determination.

FoundModulus – Modulus of foundation.

CARD 12:

NPRNT – Flag for printing. Set to 1 if stiffness matrices are to be printed.

NSPV – Number of displacement boundary conditions.

NumConcentLoads – Total number of concentrated forces in the plate. Note: in dynamic analysis, NumConcentLoads must be set equal to zero, because dynamic analysis cannot be run with concentrated loads.

CARD 13: – (Note: Skip this card if NSPV=0)

IPV(I), (I=1,NSPV) – Degrees of freedom of displacement boundary conditions.

VPV(I), (I=1,NSPV) – Values of displacement boundary conditions.

CARD 14: – (Note: Skip this card if NumConcentLoads=0)

nFxElemNo(I) – Element number where concentrated force is applied.

FxLocation(I) – Location of concentrated force from Node I of element.

FxMag(I) – Magnitude of concentrated force. Note: provide 1 line of data of nFx-ElemNo(I), FxLocation(I), FxMag(I) for each concentrated force.

CARD 15†: – (Note: Skip this card if type of analysis is different than transient)

Gamma – Gamma factor of Newmark's method.

Beta – Beta factor of Newmark's method.

DeltaT – Time increment.

TotalTime – Total time for which transient analysis is carried out.

DispInit – Initial displacement (t=0.0 sec).

VelocityInit – Initial velocity (t=0.0 sec).

Alpha1 – Constant used in proportional damping matrix.

Alpha2 – Constant used in proportional damping matrix.

CARD 16: – (Note: skip this card if type of analysis is eigenvalue)

NodeX – Node where displacements are desired.

XPoint – x-coordinate of point where stresses are printed.

ZPoint – Depth coordinate of location where stresses are printed.

A.2 Sample Input File

This input file is for Specimen 1, $[90/0/90]_T$ Layup. Loads P/2 in Card 14 are iteratively chosen such that the finite element output indicates structural failure.

```
CARD 01:  8 3 1431.7 1.45E-4 0

CARD 02:  162.E9 9.7E9 9.7E9 5.9E9 5.9E9 2.0E9 0.3 0.3 0.5

CARD 03:  2.618E9 1.620E9 66.E6 248.E6 66.E6 248.E6 103.E6 103.E6 77.E6 90 0 90 90 0 90

CARD 04:  10 469.42 1.39E-2

CARD 05:  1.056E9 1.114E9 0.379E9 587.9E6 587.9E6 587.9E6 0.25 0.25 0.25

CARD 06:  8.86E6 8.86E6 10.3E6 10.3E6 4.38E6 4.38E6 2.8894E6 2.8894E6 2.8894E6

CARD 07:  1 0.1524 0.025811 20

CARD 09:  0.0 0.0 0.1524

CARD 10:  0.0 1e10 0.0

CARD 11:  0.001 0.01 0.5 0

CARD 12:  0 2 2

CARD 13:  1 101 0.0 0.0

CARD 14:  6 0.0  -6.64E2

CARD 14:  16 0.0 -6.64E2

CARD 16:  11 0.01 0.001
```

Appendix B. Additional Photographs of Sandwich Beam Failure

Presented in this appendix are additional photographs of the specimens taken after the sandwich beams exhibited structural failure.

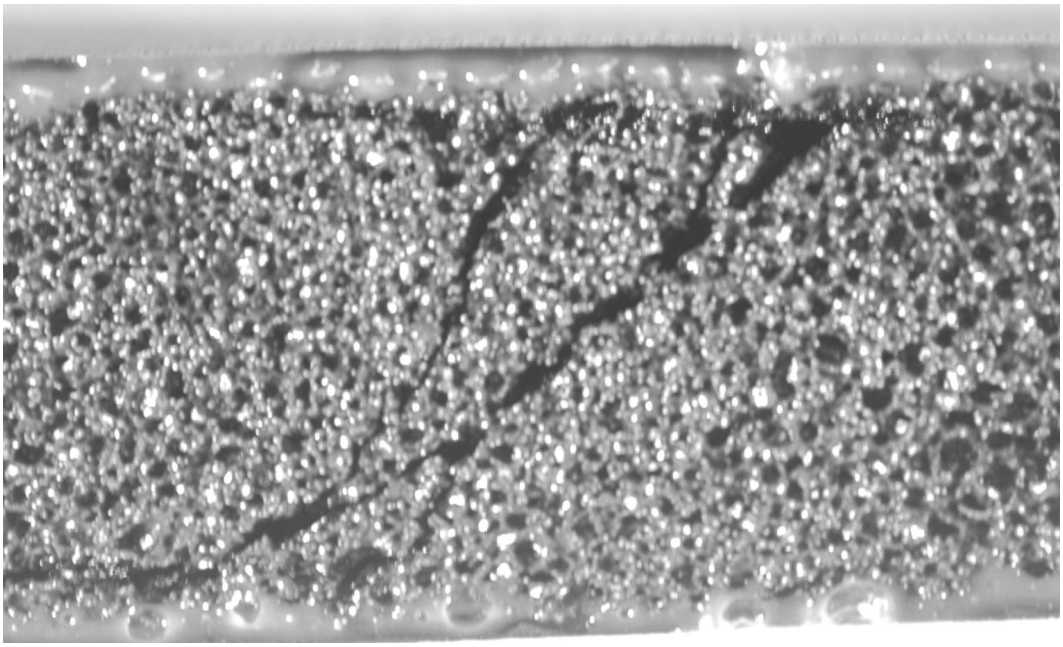

Figure B.1 Sandwich Beam Failure (5×) (Specimen 4)

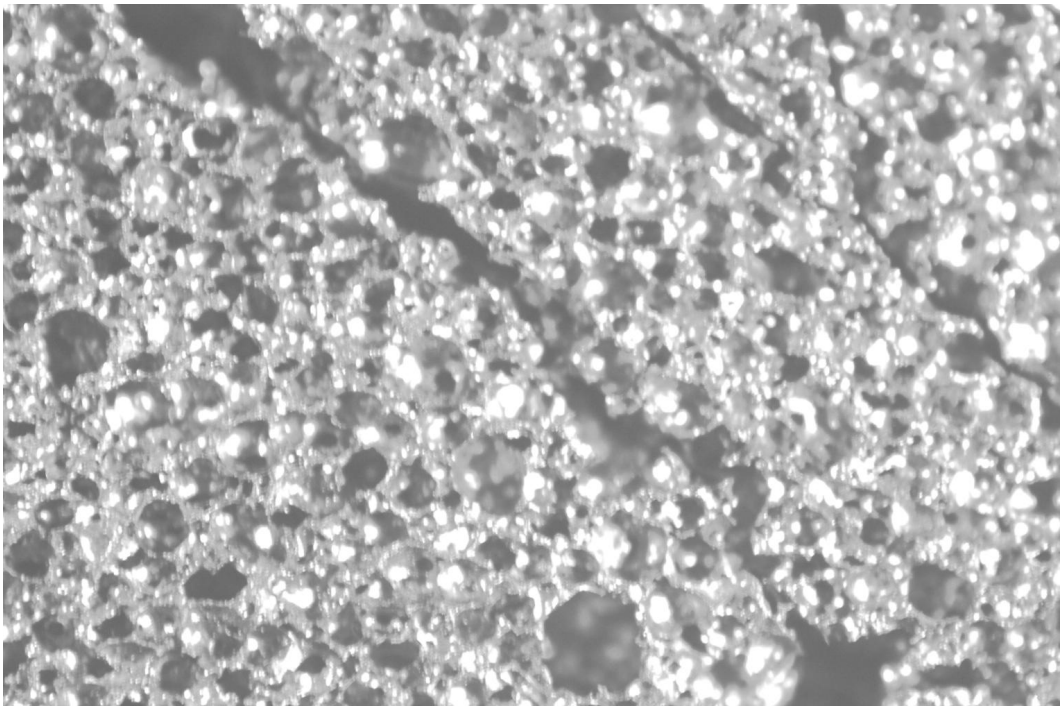

Figure B.2 Sandwich Beam Failure (10×) (Specimen 4)

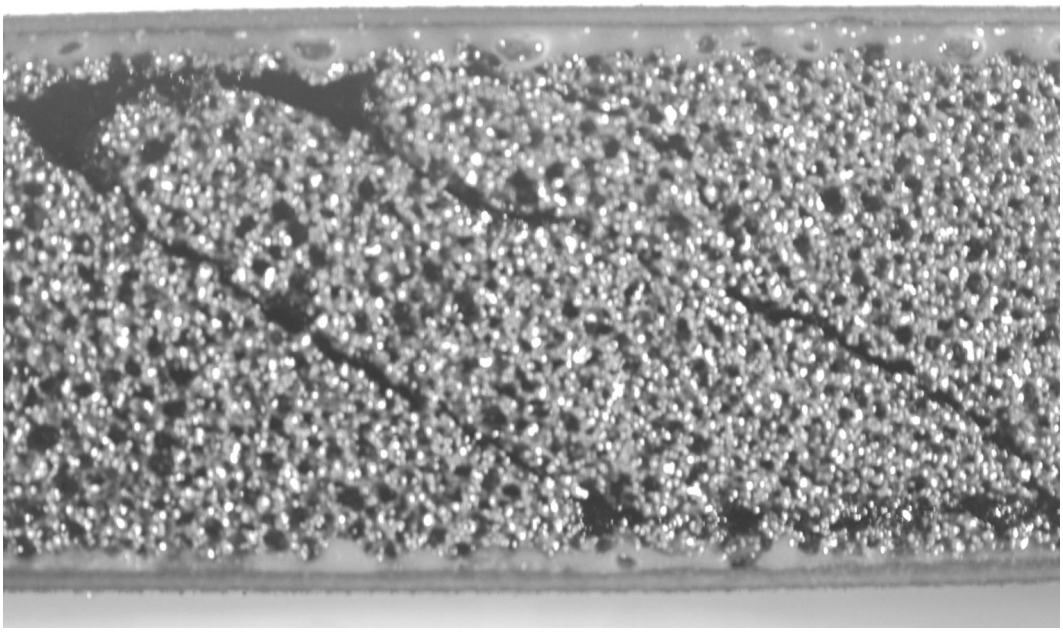

Figure B.3 Sandwich Beam Failure (5×) (Specimen 6)

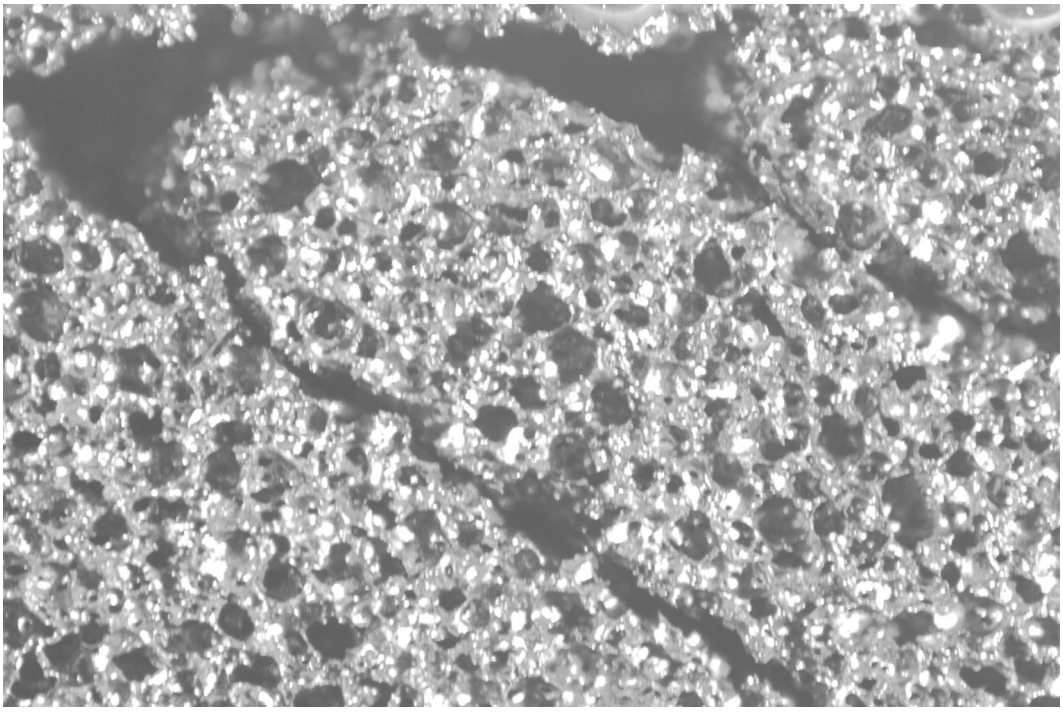

Figure B.4 Sandwich Beam Failure (10×) (Specimen 6)

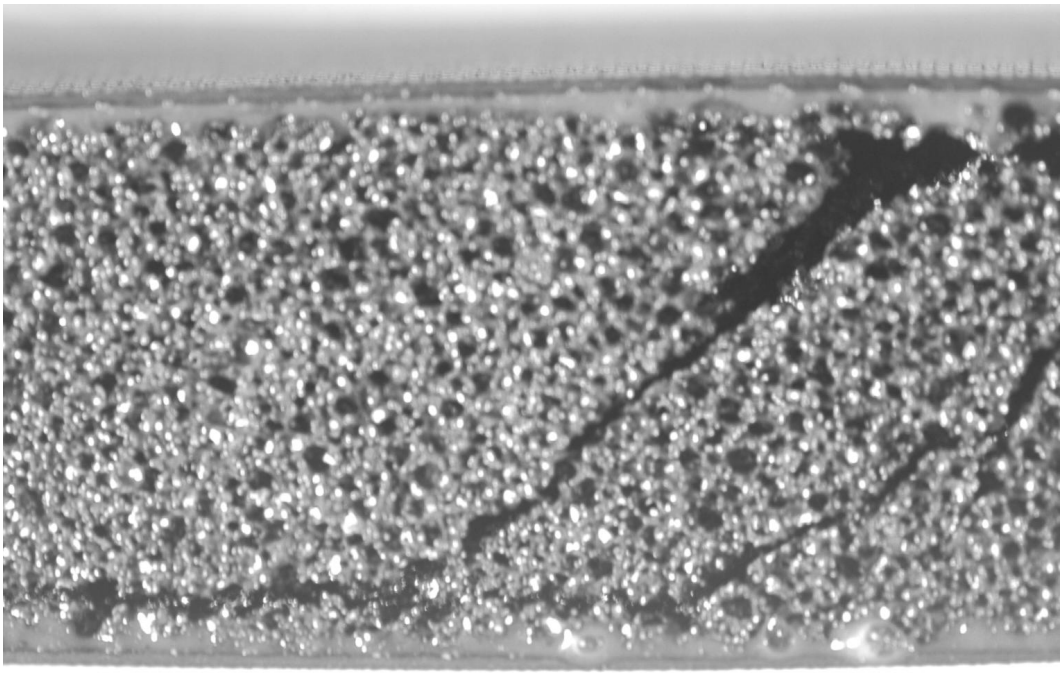

Figure B.5 Sandwich Beam Failure (5×) (Specimen 7)

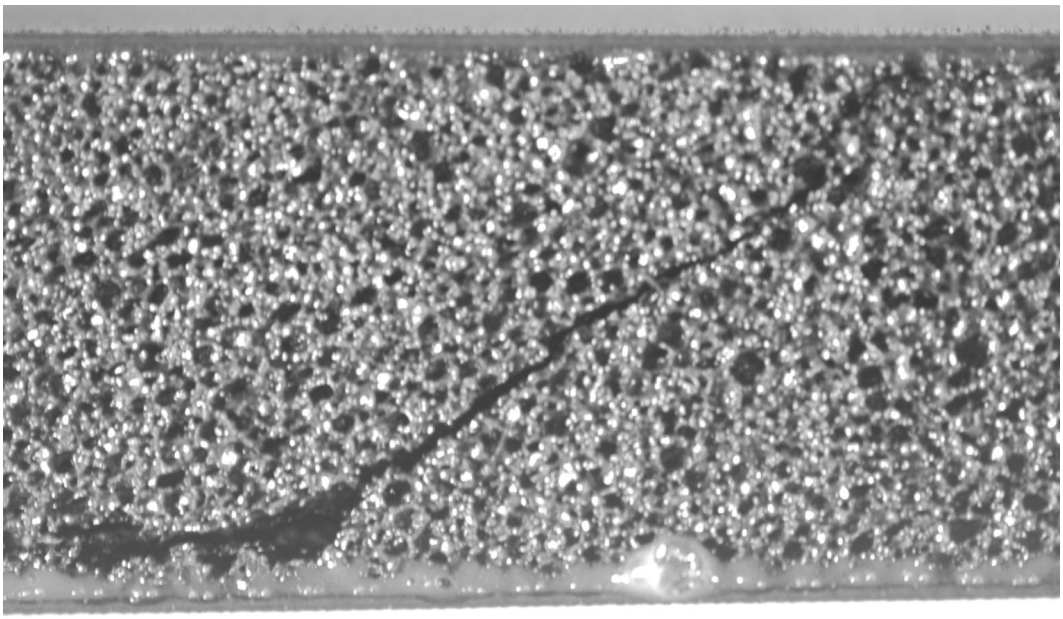

Figure B.6 Sandwich Beam Failure (5×) (Specimen 8)

Vita

First Lieutenant Troy C. Welker was born in La Crosse, Wisconsin. He graduated from Immanuel Lutheran High School in Eau Claire, Wisconsin, in May 1995. He then entered undergraduate studies at the University of Minnesota in Minneapolis, Minnesota, where he graduated with a Bachelor of Aerospace Engineering and Mechanics degree *cum laude* in March 1999. He was commissioned through the University of Minnesota Air Force ROTC program in June 1999.

Lieutenant Welker's first assignment was as a maintenance officer in the 314th Airlift Wing, Little Rock Air Force Base, Arkansas, where he held flight commander positions in the 62d Airlift Squadron and 314th Maintenance Squadron. While stationed at Little Rock Air Force Base, Lieutenant Welker pursued graduate study at the University of Arkansas in Fayetteville, Arkansas, where he earned a Master of Science degree in Operations Management in August 2001. His next assignment was as a student in the Graduate School of Engineering and Management at the Air Force Institute of Technology.

Upon graduation, Lieutenant Welker will be assigned as Chief Engineer and Program Manager, Aircraft Battle Damage Repair Program Office, Wright-Patterson Air Force Base, Ohio.

Bibliography

1. Agarwal, Bhagwan D. and Lawrence J. Broutman. *Analysis and Performance of Fiber Composites* (Second Edition). New York: John Wiley & Sons, Inc., 1990.
2. Allen, Howard G. *Analysis and Design of Structural Sandwich Panels*. Oxford, United Kingdom: Pergamon Press Ltd., 1969.
3. Bažant, Zdeněk P. and others. "Size Effect in Fracture of Sandwich Structure Components: Foam and Laminate." *Proceedings of the 2001 ASME International Mechanical Engineering Congress and Exposition*. Number IMECE2001/AMD-25413. 1–12. New York: American Society of Mechanical Engineers, 2001.
4. Cook, Robert D. and others. *Concepts and Applications of Finite Element Analysis* (Fourth Edition). New York: John Wiley & Sons, Inc., 2002.
5. Cytec Engineered Materials Inc. *CYCOM 5250-4 Prepreg System*. Technical Datasheet 012102. Technical Service, Anaheim, California, January 2002.
6. Dai, J. and H.T. Hahn. *Failure of Resin Transfer Molded Sandwich Beams in Flexure*. Grant N00014-99-4-0798, Los Angeles: University of California, Los Angeles.
7. Daniel, Isaac M. and others. "Core Failure Modes in Composite Sandwich Beams." *Proceedings of the 2001 ASME International Mechanical Engineering Congress and Exposition*. Number IMECE2001/AMD-23776. 293–303. New York: American Society of Mechanical Engineers, 2001.
8. Falk, Lars. "Foam Core Sandwich Panels With Interface Disbonds," *Composite Structures*, *28*:481–490 (1994).
9. Hashin, Zvi. "Failure Criterion for Unidirectional Fiber Composites," *Journal of Applied Mechanics*, *47*:329–334 (1980).
10. Herakovich, Carl T. *Mechanics of Fibrous Composites*. New York: John Wiley & Sons, Inc., 1998.
11. Herup, Eric J. and Anthony N. Palazotto. "Low Velocity Impact Damage Initiation in Graphite/Epoxy/Nomex Honeycomb-Sandwich Plates," *Composites Science and Technology*, *57*:1581–1598 (1997).
12. Kopka, Helmut and Patrick W. Daly. *A Guide to LaTeX* (Third Edition). Harlow, United Kingdom: Addison Wesley Longman Limited, 1999.
13. Nemes, J.A. and K.E. Simmonds. "Low Velocity Impact Response of Foam-Core Sandwich Composites," *Composite Materials*, *26*(4):500–520 (1992).
14. Palazotto, Anthony N. and others. "Low Velocity Impact Damage Characteristics of Z-Fiber Reinforced Sandwich Panels—An Experimental Study," *Composite Structures*, *43*:275–288 (1999).

15. Palazotto, Anthony N. and others. "Finite Element Analysis of Low-Velocity Impact on Composite Sandwich Plates," *Composite Structures, 49*:209–227 (2000).

16. Palazotto, Anthony N. and Victor Y. Perel. "Consideration of Through the Thickness Strains for a Sandwich Panel." Presentation based on [19], 2001.

17. Perel, Victor Y. *Three-Dimensional Dynamic Stress Analysis of Sandwich Panels*. PhD dissertation, Graduate School of Engineering and Management, Air Force Institute of Technology (AETC), Wright-Patterson AFB OH, June 2000.

18. Perel, Victor Y. "A Layerwise Model of a Sandwich Plate in Cylindrical Bending with a Rigid Body on its Upper Surface, Dropped on Elastic Winkler Foundation." Brief description included with finite element code, 2001.

19. Perel, Victor Y. and Anthony N. Palazotto. "Finite Element Formulation for Cylindrical Bending of a Transversely Compressible Sandwich Plate, Based on Assumed Transverse Strains," *International Journal of Solids and Structures, 38*:5373–5409 (2001).

20. Perel, Victor Y. and Anthony N. Palazotto. "Finite Element Formulation for Thick Sandwich Plates on an Elastic Foundation," *AIAA Journal, 40*(8):1627–1637 (August 2002).

21. Perel, Victor Y. and Anthony N. Palazotto. "Dynamic Geometrically Nonlinear Analysis of Transversely Compressible Sandwich Plates," *International Journal of Nonlinear Mechanics, 38*:337–356 (2003).

22. Popov, Egor P. *Introduction to Mechanics of Solids*. Upper Saddle River, New Jersey: Prentice-Hall, Inc., 1968.

23. Saada, Adel S. *Elasticity: Theory and Applications* (Second Edition). Malibar, Florida: Krieger Publishing Company, 1993.

24. Sihn, Sangwook and Brian P. Rice. "Sandwich Construction with Carbon Foam Core Materials," *accepted for publication to Journal of Composite Materials* (2002).

25. Sihn, Sangwook and Ajit K. Roy. "Modeling and Stress Analysis of Open-Cell Carbon Foam," *submitted for publication to Journal of the Mechanics and Physics of Solids* (2002).

26. Song, Yuzhao and Ziqi Chen. "A Bodner Type of Material Model for the Description of Foam Properties." *Proceedings of the 2001 ASME International Mechanical Engineering Congress and Exposition*. Number IMECE2001/AMD-23769. 225–230. New York: American Society of Mechanical Engineers, 2001.

27. Tsai, Stephen W. and Edward M. Wu. "A General Theory of Strength for Anisotropic Materials," *Composite Materials, 5*:58–80 (1971).

28. Ugural, Ansel C. and Saul K. Fenster. *Advanced Strength and Applied Elasticity* (Third Edition). Upper Saddle River, New Jersey: Prentice-Hall, Inc., 1995.

29. United States Air Force Museum. Dayton, Ohio: Wright-Patterson Air Force Base, 2003.

30. Whitney, James M. *Analytical Mechanics of Composite Materials*. Dayton, Ohio: Published by author for use as course text, 2002.

REPORT DOCUMENTATION PAGE

Form Approved
OMB No. 0704–0188

1. REPORT DATE *(DD–MM–YYYY)*	2. REPORT TYPE	3. DATES COVERED *(From — To)*
25–03–2003	Master's Thesis	Sep 2001 — Mar 2003

4. TITLE AND SUBTITLE

EXPERIMENTAL AND COMPUTATIONAL FAILURE ANALYSIS OF GRAPHITE/BISMALEIMIDE LAMINATED COMPOSITE AND CARBON FOAM IN SANDWICH CONSTRUCTION

5a. CONTRACT NUMBER

5b. GRANT NUMBER

5c. PROGRAM ELEMENT NUMBER

6. AUTHOR(S)

Welker, Troy C., First Lieutenant, USAF

5d. PROJECT NUMBER

5e. TASK NUMBER

5f. WORK UNIT NUMBER

7. PERFORMING ORGANIZATION NAME(S) AND ADDRESS(ES)

Air Force Institute of Technology
Graduate School of Engineering and Management
2950 P Street, Building 640
WPAFB OH 45433-7765

8. PERFORMING ORGANIZATION REPORT NUMBER

AFIT/GAE/ENY/03-10

9. SPONSORING / MONITORING AGENCY NAME(S) AND ADDRESS(ES)

AFRL/VASM
Attn: Mr. Mark M. Derriso
2210 8th Street, Building 146
WPAFB OH 45433-7510

10. SPONSOR/MONITOR'S ACRONYM(S)

11. SPONSOR/MONITOR'S REPORT NUMBER(S)

12. DISTRIBUTION / AVAILABILITY STATEMENT

APPROVED FOR PUBLIC RELEASE; DISTRIBUTION UNLIMITED.

13. SUPPLEMENTARY NOTES

14. ABSTRACT

Sandwich beams consisting of a carbon foam core and graphite/bismaleimide face sheets were constructed and tested. Nine specimens were fabricated, using three distinct cross-ply symmetric face sheet layups with a constant core thickness. Four-point bend testing, controlled by a constant rate of midspan vertical displacement, was used to load the specimens to failure. Displacements and strains from the experiment were compared to analytical sandwich beam theory, and displacements and failure loads were compared to a layerwise finite element solution. A phenomenological failure criterion was developed that compares favorably with experimental failure data. The finite element solution gives failure within an average of 7.58% of experiment, and a stiffness within an average of 11.16%. The analytical sandwich beam theory predicts stiffness within 4.83% of experiment, and strain within 5.27% of experiment. This research shows that the finite element theory has the ability to predict failure onset and location in a sandwich structure, and that the face sheet layups with higher stiffness delay the onset of shear failure in the core.

15. SUBJECT TERMS

finite element analysis; sandwich construction; fiber reinforced composites; graphitic foam

16. SECURITY CLASSIFICATION OF:			17. LIMITATION OF ABSTRACT	18. NUMBER OF PAGES	19a. NAME OF RESPONSIBLE PERSON
a. REPORT	b. ABSTRACT	c. THIS PAGE			Anthony N. Palazotto, PhD, PE (ENY)
U	U	U	UU	91	19b. TELEPHONE NUMBER *(include area code)* (937) 255–3636, ext 4599